

# NGP A stars – density variation, kinematics and the total mass density of the disk

**J. Knude**

Niels Bohr Institute for Astronomy, Geophysics and Physics, Juliane Maries Vej 32, DK-2100 København Ø, Danmark (indus@astro.ku.dk)

Received 23 August 1996 / Accepted 26 May 1997

**Abstract.** From an uvby $\beta$  photometric survey of the north galactic pole where most A stars (A3 – A9) above  $b = 70^\circ$  and brighter than  $B = 11.5$  were included we report the *observed* number density and age variation with  $z$ (pc). Stars between  $\sim 30$  and 1300 pc are included.

Our sample consists of 396 sharply defined main sequence/subgiant A stars following the Strömberg – Crawford definition, no B, imA or F type stars are included, approximate color limits are 0.055 – 0.220 in  $(b-y)_0$ . Proper motions from the PPM and CAMC catalogs are available for all stars implying U and V velocities. Radial velocities for a subsample (179 stars with  $b \geq 75^\circ$  and  $z \leq 450$  pc) are available from the literature. From a luminosity point of view the sample is volume complete within  $\sim 450$  pc.

For a fit to the observed density variation the choice of function is not obvious and it seems that these A stars may not be fitted by a single law but requires at least two and more likely up to four components. Assuming exponential density variation two groups of stars seem present with scale heights around 65 and 165 pc respectively. The latter may be an underestimate due to volume incompleteness for the coolest unevolved A stars beyond 450 pc. The exponentials approximating the number density has a relative normalization 1.00: 0.03 for  $z = 0$  pc. With these two components only the first of Perry's (1969)  $h = 40$  and  $h = 600$  pc groups seem represented in our volume complete sample. Adopting instead a gaussian variation the data may indicate three components with scale heights 45, 75 and 155 pc and relative normalization 1.0:0.5:0.2, respectively. Finally a set of four  $\text{sech}^2(\frac{z}{h})$ s with scale heights 55, 85, 165 and 420 pc and relative normalizations 1.00:0.47:0.18:0.005 for  $z = 0$  seem to fit the number density data well. This combination is based on independent 75 pc bins. A  $\text{sech}^2$  variation is perhaps the most obvious choice being the expected variation for an isothermal and selfgravitating disk.

With a 100 pc running binning there are indications that the stars older than the sample median 0.75 Gyr require a component with a scale height 680 pc. It may also be present in the young sample, ages less than 0.75 Gyr, but only beyond  $\sim 400$  pc. What perhaps is more surprising is the formal presence of groups of stars displaying a density maximum at  $z = 200 - 250$  pc,

present for both age groups, and most interestingly the angular momentum also displays irregularities at the same  $z$  distances. The hump is not proposed to represent a physical entity but something like it is required for fitting the observations better than 10%. A consequence of the hump is that derivatives of the distribution display large variations. There seems to be significant differences between this distribution and the sum of four  $\text{sech}^2$ s from the previous paragraph.

W and U dispersions seem to have a constant ratio within the  $z$  range where we have both kinds of data.  $\sigma_U$  shows a homogeneous increase from  $\sim 20$  to 45  $\text{km s}^{-1}$  within the completeness limit, with a 75 pc independent binning, and to  $\sim 70$   $\text{km s}^{-1}$  at 800 pc. The complete U histogram may not be fitted with a single gaussian, three with different dispersions and mean values provide a reasonable fit. A more detailed binning shows  $\partial\sigma_U/\partial z$  to change in a discontinuous way at  $\sim 200$  pc.

An application of the data might be a combination of the density and velocity data for a determination of the local, total disk density. But since velocity dispersions do obey some sort of age dependence the age -  $z$  variation turns out to be of importance and there is a very clear systematic trend of mean ages with  $z$ . The average age increases almost linearly to  $\sim 0.75$  Gyr, reached at 200 pc, and then it stays constant within the completeness limit. On the average the younger A stars show a relative absence beyond 200 pc implying that very different velocity dispersions might be seen on either side of 200 pc.

The curve fitted to the density data permits a study of its derivatives. Adopting a linear approximation to  $\sigma_W$ 's  $z$  variation, instead of isothermallity,  $\partial K_z/\partial z$ 's variation within  $\sim 150$  pc indicates that the combined Poisson – Jeans equation may only return estimates of the local volume mass density that vary within a factor of two but the fit by four  $\text{sech}^2$ s turns out to be equivalent with a representation by two gaussians with scale heights 129 and 250 pc which implies that between 100 and 200 pc  $\rho_{total} = 0.12 \pm 0.04 \mathcal{M}_\odot \text{pc}^{-3}$  whereas  $\partial K_z/\partial z$  from the same fit and a linear approximation to the  $\sigma_W - z$  variation returns  $\rho_{total}(z \approx 0) \approx 0.05 \mathcal{M}_\odot \text{pc}^{-3}$ .

The age, density and kinematic inhomogeneities revealed in the sample compel us to the conclusion that the A stars do not

trace the galactic potential in a simple way – probably because the age mixing varies with distance.

**Key words:** galaxy: kinematics and dynamics – solar neighbourhood – stellar content – structure

## 1. Introduction

An essential issue for the Milky Way and for spirals in general is the form of the light and mass variation perpendicular to the disk and the question of isothermality. Whether the stellar distribution may be characterized by just one kinematic group or consists of several, individually isothermal groups. The combination of the density variation and the vertical kinematics may, within the framework of suitable models and assumptions, provide an estimate of the total density in the disk and bear on the important question of the existence of any unidentified matter in the disk. Some edge on spirals show indications of a surface brightness following a  $\text{sech}^2$  variation perpendicular to the disk, van der Kruit and Searle (1981), van der Kruit (1988), and maybe even bear the imprint of several components, Dove and Thronson (1993), Just et al (1996). In the Milky Way counts of polar A stars may possibly be used to study similar problems but since they are relatively young they might have problems with an immature phase mixing but could conversely bear on the question of recent merging processes, Lance (1988), Preston, Beers and Shectman (1994) and maybe even help identifying stars belonging to groups homogeneous in some respect like age, metallicity and kinematics. Moreover with A stars in the Milky Way we are in a position to indicate  $z(\text{pc})$ , age, mass and a rough  $[\text{Fe}/\text{H}]$  for individual stars from photometry alone and thus try entangling various components. At latitudes above  $70^\circ$  the photometric distance and proper motions alone provide  $U$  and  $V$  motions and we may conduct a combined study of the density laws and part of the kinematics.

Traditionally A stars have been used for tracing the local galactic potential, Perry (1969), Hill, Hilditch and Barnes (1979), Lance (1988). With similar luminosities as K giants main sequence A stars of even modest apparent magnitude are useful and cover a  $z$  range of some hundred pc and the present sample's limiting magnitude even permit detection of As from the upper part of the main sequence slightly beyond 1 kpc. Our relatively bright sample of A stars mainly bears on the solar neighborhood and less on the distant A stars discussed by Lance (1988), Rodgers and Roberts (1993a, 1993b) but since  $1200 \text{ } \square^\circ$  has been surveyed some of these high velocity population I A stars should be present. The resulting A stars are all younger than 1.7 Gyr with a median age 0.75 Gyr comparable to the age of the Hyades. Ages are based on the  $\beta$ ,  $c_0 - \log g$ ,  $T_{\text{eff}}$  calibration by Moon and Dworetzky (1985), Dworetzky and Moon (1986), and the Yale isochrones, Green, Demarque and King (1987).

With a median age like the Hyades' one might expect some resemblance in the  $z$  – distribution of our sample and that of

the galactic clusters, Friel (1995). It turns out that the age is a most important parameter. The exponential scale height of 55 pc found for open clusters younger than the Hyades may thus be compared to that of a group in the present sample, those following  $\text{sech}^2(\frac{z}{55})$ , whereas the exponential scale height of 375 pc valid for open clusters older than the Hyades might have a counterpart in  $\text{sech}^2(\frac{z}{420})$  dominating beyond  $\sim 400$  pc.

Previous studies of the NGP (Perry (1969)), the SGP (Lance (1988)) and of the galactic clusters indicate a density variation that may be adopted by a sum of only two exponentials, presently we discuss that a sum of more than two  $\text{sech}^2(\frac{z}{h})$  may be a better fit for the NGP A stars at least. Recently Gould, Bahcall and Flynn (1996) suggest M dwarfs to obey a sum of one  $\text{sech}^2$  and an exponential with a scale height 656 pc.

A final determination of the local disk density seems, however, to be impossible from our rather complete data set complying with most of the demands suggested by Gildea and Bahcall (1985) and by Gould (1990). Only data missing are RV for  $\sim 200$  stars but 50% do have radial velocities. In their discussion of sampling errors Gildea and Bahcall (1985) propose that the time for initial fluctuations to decrease to a steady state is a few passages through the mid plane, some hundred million years probably. The sample, however, seems to undergo significant changes at about 200 pc. Volume completeness is a necessary but not a sufficient requirement, what proves more essential turns out to be an identical age mixture as a function of  $z$  distance and this is a condition that the A stars cannot meet.

## 2. Sampling

### 2.1. A star definition

The sample comprises about 12% of an uvby $\beta$  survey of “all” A and F stars at the NGP. The observed cone with opening angle  $20^\circ$  is common for all magnitudes. Programme stars are reduced to the standard system from observations of a rather large set of standards. Details of the definition of A stars intrinsic indices may be found in Strömgren (1966) and Crawford (1979). Note that their A definition does not include A0 or earlier and that we exclude the intermediate group A stars A1 – A2, mainly because they were not included in the original spectral type classification (T. Oja, personal communication) but also because they are less accurately calibrated than later As. So we don't benefit from the imAs larger luminosity. As discussed below imA has been included in previous investigations which may have caused some confusion when resulting scale heights are compared. 35 marginal imA stars are present in the NGP survey – but as already mentioned they are not included. We do, however, include the metallic line A stars,  $-0.050 \leq \delta m_0(\beta) \leq -0.025$ , since the controversy on their  $\log(g)$  seems to have reached a conclusion, Smalley and Dworetzky (1993). Metal weak stars with  $\delta m_0(\beta) \lesssim 0.04$  are also retained in the sample, they are few anyway. The metallicity may be considered as solar with a median  $\delta m_0(\beta) = 0.006$ . Furthermore we assume that  $\delta c_0(\beta)$  variations exclusively are due to different  $\log(g)$ s and do not depend on rotation, Gray (1989). In addition to Crawford's upper  $\delta c_0(\beta)$  limitation

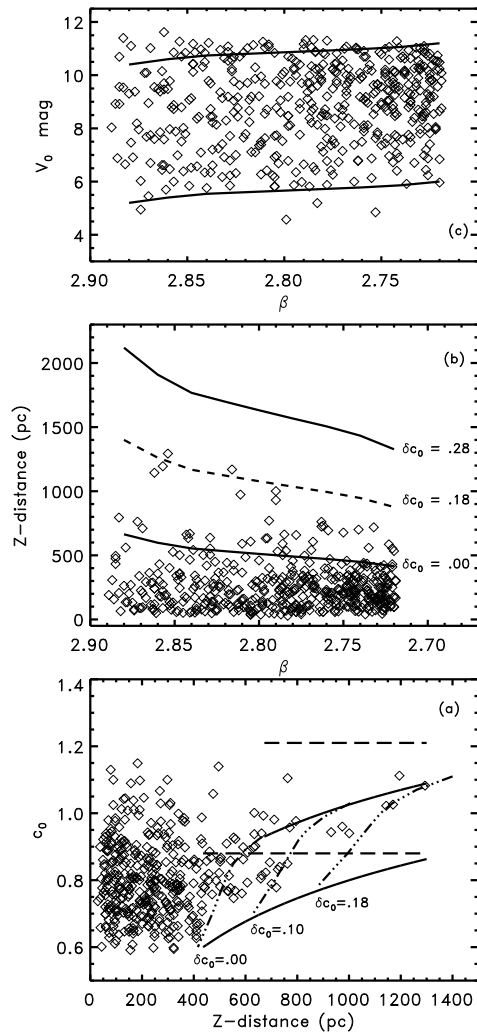


**Fig. 1a–c.** Curves assume  $A_V = 0$ . Data points are individually corrected for reddening. **a**  $c_0$  vs.  $z$ (pc) diagramme. Solid curves start at distances where unevolved  $\beta = 2.880$  (upper end) and  $\beta = 2.720$  (lower end) are just included. Note that since the sample is limited by  $B = 11.5$ , the limiting  $V$  magnitude depend on color. These distances are 673 and 450 pc respectively. The three curves connecting the two solid curves are computed for constant evolution,  $B_0 = 11.5$  and  $(b-y)_0$  varying from 0.066 (upper) to 0.226 (lower). The dashed curves indicate maximum  $c_0$  for  $\beta = 2.880$  (upper) and  $\beta = 2.720$  (lower) stars. **b**  $\beta$  vs.  $z$ (pc). Lower solid curve indicates maximum distance where unevolved stars are included. Upper curve maximum distance where maximum evolved main sequence – subgiant A stars are included. Dashed curve has  $\delta c_0 = 0.180$ . All three curves have  $B_0 = 11.5$ . **c**  $\beta$  vs.  $V_0$ . Solid curves are the  $\beta - M_V$  standard line shifted +2.9 (lower) and +8.1 (upper), the latter corresponding to the samples limit for volume completeness of 450 pc

we apply a lower  $\delta c_0(\beta)$  confinement at -0.030, this in fact excludes quite a number,  $\sim 60$ , of slightly subluminous A stars. Subgiants are included in the density and dispersion discussion within the volume completeness limit.

The question of including subgiants, found by Kuijken and Gilmore (1989) to be a major error source for  $\rho_{total}(z=0)$  based on published F star data is addressed in Sect. 6.

## 2.2. Distance sampling

Some sort of completeness is of course required for a study of the density variation and it is mainly determined by the limiting magnitude and the allowed  $M_V$  variation in the main sequence/subgiant band. Along the A star standard curve  $M_V(\beta, \delta c_0 = 0)$  ranges from 2.30 to 3.10 and at any  $\beta$  the width of the main sequence is about 2.5 magnitudes corresponding to the maximum permitted  $\delta c_0(\beta)$  value of 0.280. RR Lyr stars (4), blue HBs (also 4) are present in the sample but are excluded on the maximum  $\delta c_0$  criterion. The permitted  $\delta c_0(\beta)$  range is not populated homogeneously, as noted from the  $(b-y)_0 - c_0$  or  $\beta - c_0$  diagrams (not shown). The bulk of stars have  $\delta c_0(\beta) \lesssim 0.180$ , almost no stars are located between  $c_0(\delta c_0 = 0) + 0.180$  and  $c_0(\delta c_0 = 0) + 0.280$ . The scarcity of stars with  $\delta c_0(\beta)$  between 0.180 and 0.280 may tell something about the duration of the subgiant phase in the A stars' temperature range. Consequences of this fact show up in Fig. 1a. With the limiting  $B = 11.5$  the complete A temperature range is not included at all distances. Fig. 1a is a demonstration of this. Curves in Fig. 1 are based on the A star standard table from Crawford (1979) and the assumption that  $A_V \approx 0$ . The average visual absorption in the polar cap is  $A_V \approx 0.07$ , Knude (1996). The two solid curves are loci for the minimum  $c_0$  that will be included at a given distance for  $\beta = 2.880$  (upper) and  $\beta = 2.720$  (lower) for stars with the limiting magnitude. The diagram thus includes all states of accepted A star evolution. Generally we miss the cool lesser evolved A stars beyond  $z \approx 450$  pc. *Within this distance the sample is volume complete.* Beyond 673 pc, the distance within which the unevolved  $\beta = 2.880$  stars are volume complete – and so are the evolved  $\beta = 2.880$  ones of course, the sample consists exclusively of evolved main sequence/subgiant stars and we cannot tell the volume density in detail – unless the A star luminosity function was known not to vary with  $z$ . Beyond 450 pc we might have corrected for the Malmquist bias by assuming the validity of the  $M_V$  distribution as observed within 450 pc. But we have chosen not to base our curve fitting on statistically corrected data, the high altitude A star luminosity function may differ from the local one. Fig. 1c and 1b demonstrate how  $V_{0,lim}$  varies with  $\beta$  and how the maximum detection distances vary with  $\beta$  for various stages of evolution.

If we consider the lower solid curve of Fig. 1a it shows that the coolest A stars on the standard line may be detected to  $\sim 450$  pc and not beyond since  $c_0(\delta c_0 = 0) = 0.600$  for  $\beta = 2.720$ . A stars with  $\beta = 2.720$  more distant than the 440 pc must accordingly be evolved to be included in the sample. At 1300 pc the  $\beta = 2.720$  stars reach their maximum main sequence(subgiant)  $c_0$  value:  $0.600 + 0.280$ . The dashed horizontal line indicates the maximum  $c_0$  main sequence(subgiant) value for the coolest stars. If present the evolved late As would have been included between the dashed line and the lower solid curve. Secondly the region confined by the two upper curves, corresponding to  $\beta = 2.880$  indicating the blue limit of our A star range, point out the required  $c_0$  values as a function of distance for the hottest stars to be included in the  $B \leq 11.5$  sample.

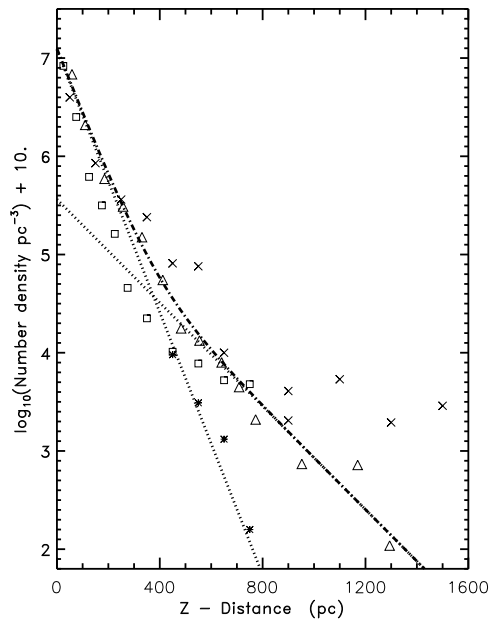


**Fig. 2.** This is the  $\log_{10}\nu(z) - z(\text{pc})$  diagramme for various samples. Boxes Perry(1969), crosses Lance(1988), triangles this paper. \*s are Perry(1969) corrected for stars that are not As in the sense of the present paper. Dotted lines are exponentials with scale heights 65 and 165 pc respectively and the dash dot curve is their sum with a relative normalization 1.00:0.03 at  $z=0$

The lower envelope of the data points in Fig. 1a may be characterized by a steep edge rising from about  $(z, c_0) = (400, 0.600)$  to  $(500, 0.750)$  followed a more shallow variation to  $(1300, 1.100)$ . Can this be understood? Partly. Instead of keeping the color (or  $\beta$ ) constant and letting the evolution vary we could ask what the  $z - c_0$  variation would look like for a constant evolution but varying color. At the limiting magnitude of course. First we keep  $\delta c_0 = 0$ , since  $B_{limit} = 11.5$  we must change  $V_{0,limit}$  according to the color. We have used  $(B-V)_0 = 1.35(b-y)_0$ , simply applying the reddening ratio of the Johnson and Strömgren systems,  $E(B-V) = 1.35 E(b-y)$ . 1.35 does not deviate much from measured values, 1.51 was found in a study of E region A and F stars (H. Jönch-Sørensen, personal communication). We see that the  $(400, 0.600) - (500, 0.750)$  edge is nicely approximated by the curve pertaining to stars with no evolution and at the limiting magnitude. As it must the  $\delta c_0 = 0$  curve connects the solid curves computed for the coolest and hottest stars where they have  $\delta c_0 = 0$ . Similarly the  $z - c_0$  variation is shown for  $\delta c_0 = 0.180$ . As the diagram shows a curve for  $\delta c_0 = 0.280$  is not required. The  $\delta c_0 = 0.180$  curve very nicely includes three of the most distant stars.

Fig. 1b gives perhaps a clearer impression of the sample completeness and state of evolution by indicating the observable  $z$  range for the A star  $\beta$  interval. The lower solid curve indicates maximum distances within which an unevolved,  $\delta c_0 = 0$  and  $B_0 = 11.5$ , star is included and the upper curve similarly the distance to which a maximum evolved main sequence(subgiant) star,  $\delta c_0 = 0.280$ , would be in the sample. The maximum distances are computed from the A star standard table,  $B_0 = 11.5$  and  $V_0 = B_0 -$

$1.35(b-y)_0$ . In Fig. 1c the upper solid curve is the  $V_0 - \beta$  relation at a distance  $\sim 450$  pc for  $B_{0,limit} = 11.5$ . The hotter A stars may thus be detected to larger distances not only because they are intrinsically brighter by  $0.8^m$  but also because their limiting  $V_0$  is  $\approx 0.5$  magnitude fainter than for the coolest A stars.

In Fig. 1b is also shown where  $\delta c_0 = 0.180$  and  $B_0 = 11.5$  stars are located. The most distant stars cluster along this curve. For  $\beta < 2.79$  the sample does not contain stars with  $B_0 = 11.5$  and  $\delta c_0 = 0.180$ . We note a group of seven stars with  $\beta < 2.77$  and  $z > 650$  pc. A group that on closer inspection turns out to be indeed homogeneous.  $\overline{M_V} = 1.66 \pm 0.11$ ,  $\overline{\delta m_0} = 0.031 \pm 0.013$  remarkably large compared to the sample median of only 0.006.  $\overline{A} = 10.4 \pm 0.8 \cdot 10^8 \text{ yr}$ ,  $\overline{M} = 1.90 \pm 0.05 \mathcal{M}_\odot$ ,  $\overline{z} = 716 \pm 28$  pc. And for the kinematics  $\overline{U} = 31$ ,  $\sigma_U = 66 \text{ km s}^{-1}$ ,  $\overline{V} = -46$ ,  $\sigma_V = 31 \text{ km s}^{-1}$ . The ratio  $\sigma_V/\sigma_U$  has a standard relaxed value 0.47. This group is not confined to a small area but has  $\delta$  ranging from  $+13$  to  $+41^\circ$ . The metallicity is noteworthy,  $\delta m_0 = 0.031$ , almost like intermediate population II F stars. With  $\delta c_0 = 0.139 \pm 0.010$  they are not quite subgiants as discussed in Sect. 6, could they possibly be blue stragglers? From Fig. 7c we learn that this group is found on the  $\text{sech}^2(\frac{z}{680})$  component, just at the distance where the observed volume density for the stars older than  $7.5 \cdot 10^8$  yr drops off.

The seven most distant stars, those along the  $\delta c_0(\beta) = 0.180$  curve in Fig. 1b, are subgiants with the same  $\delta m_0(\beta)$  as the group at 716 pc but  $\overline{A} = 5.6 \pm 2.0 \cdot 10^8 \text{ yr}$  and  $\overline{U} = -28$ ,  $\sigma_U = 71 \text{ km s}^{-1}$ ,  $\overline{V}$  and  $\sigma_V$  equal to  $-28$  and  $14 \text{ km s}^{-1}$  respectively. The  $\sigma_V/\sigma_U$  ratio is remarkably low for such young stars. These seven stars are not suggested to form a homogeneous group. The differences between these two most remote groups illustrate how careful one must be beyond the volume completeness limit.

### 3. The $\log \nu(z) - \text{distance}$ variation

#### 3.1. The number count - $z$ -distance variation

As the previous section indicated the understanding of the sampling is intricate from statistical reasons alone. We therefore first present the simplest possible number -  $z(\text{pc})$  variation: raw counts in 75 pc independent slices. There is a reasonably number of stars in each slice within 800 pc. No stars between 800 and 900 pc. Three stars between 900 and 1000 pc and then four stars between 1100 and 1300 pc. The upper distance limit confining the volume used to compute the most remote number density is the distance to which the lone star at 1300 pc would have been included. An impression of the distance distribution may be obtained from Fig. 1a and 1b. Recall that volume completeness only pertain within  $\sim 450$  pc. The resulting number densities are presented in the  $\log_{10}(\nu) - z$  diagramme, Fig. 2. Fig. 2 also includes the work by Perry ( $\square$ ) (1969) and by Lance ( $\times$ ) (1988). Following Perry and Lance we try to adapt exponentials to the  $\log_{10}(\nu) - z$  variation. For the first 250 pc an exponential  $\exp(-\frac{z}{65})$  adapt the data well but beyond 250 pc it underestimates the number density. Densities between 450 and 1300 pc may be approximated by  $\exp(-\frac{z}{165})$ . The stars between 250 and 450 pc have not been used choosing the exponentials and may conse-

quently be used judging the goodness of the fit. The complete distance range from 50 to 1300 pc obeys the sum of these two exponentials with a relative normalization 1.00:0.03 at  $z = 0$  pc. The number of stars predicted for  $z=0$  is  $\nu_0 = 12.5 \cdot 10^{-4}$  A stars  $\text{pc}^{-3}$ , only a factor 2.5 above the canonical value for stars of spectral type A. This could be remedied by using a lower scale height than 65 pc but a consequence would be that the first distance bin would fall far from the fit, so we prefer  $h = 65$  pc to a lower value. We note that the three points between 250 and 450 fall almost exactly on the resulting curve, deviations less than 20%.

### 3.2. Perry and Lance's density – $z(\text{pc})$ variations

An early discussion of space density –  $z$  variation, for early type A dwarfs was undertaken by Perry (1969) in the earliest days of the uvby $\beta$  system, before the final distance calibrations by Crawford were ready. Stellar tracer type was selected from the objective of reaching  $z \approx 750$  pc and resulted in a brightness criterion  $M_V \lesssim +1.5$ . The boxes of Fig. 2 indicate Perry's results. Fig. 6 in Perry *op. cit.* lends more credit to the suggestion that the NGP early A dwarfs are made up from two distinct populations than does Fig. 2. The present counts are indicated by triangles. We note that Perry's space density falls below the present number density within  $\sim 700$  pc in a systematic way. The steeper variation could be caused by the choice of stellar tracer. Demanding  $M_V \lesssim +1.5$  means mainly A0 – A2 stars, earlier than our hot limit at A3 where  $M_V$  on the standard line is 2.3. Such stars are very young. The small value 40 pc for the exponential scale height may be a consequence of the choice of tracer and reflects a very young populations' response to the Galaxy's potential and heating mechanisms. Since the Perry distances are based on an early distance calibration, perhaps based on a Hyades distance modulus of 3.0, compared to the present day value of  $\approx 3.5$ , the smaller distances may be understood. We have not been able to confirm if 3.0 has been used.

Most strikingly is however the apparent protrusion of a remote population with a much larger scale height than the 40 pc from about 500 pc. Since Perry (1969) has published the individual uvby $\beta$  data for his polar A stars a detailed comparison of stars termed A stars is possible. For the stars beyond 400 pc we have gone through the photometry and applied Strömgren and Crawford's criteria as adopted in the present paper. A large part of the protrusion must consist of stars earlier than A3. The resulting number densities after correction are indicated by \*'s in Fig. 2. The point in the 700 – 800 pc bin is an arbitrary upper limit since this bin contains no late A stars in the sense of the present paper. Perry's density law is still referenced as evidence for a high  $z$  population of early type stars, Rodgers and Roberts (1993a) quotes  $\sim 45$  and  $\sim 500$  as exponential scale heights for the two Perry components, but one has to recall that it is based on A0 – A2 stars. Fig. 2 also shows the density variation found by Lance (1988) from faint SGP A stars. Lance's bin size is 100 pc increasing to 200 beyond 600 pc. The volume density presented by Lance pertain to a  $100 \square^\circ$  area, called the box, where the sample should be 98% complete to  $V \approx 14$ . Ten stars

in the box are beyond 1 kpc. Lance's A star definition follows Strömgren and Crawford but are based only on uvby photometry,  $\beta$  not being available. This could imply a possible problem since distances must be derived in quite another way than suggested by Crawford's (1979) calibration. Absolute visual magnitudes follow from masses as derived from mass tracks in  $\Theta$  – logg diagrams (Yale), masses are converted to luminosity, luminosities transformed to absolute bolometric magnitudes which with a bolometric correction give  $M_V$ 's. Lance estimates her distances to be accurate to about  $\pm 16\%$  – comparable to that of the photometric distances  $\pm 15\%$  for A stars in the Strömgren system, Knude (1978). We will not discuss this any further only mention that comparisons of uvby $\beta$  data to theoretical tracks, evolutionary and isochrones, most often requires adjustments in  $(b - y)_0$  and  $c_1$  or equivalently  $\Theta$  and logg, due to the uncertain solar color and luminosity calibrations. As an example a faint,  $V \approx 13$ , NGP sample of F stars was given in Knude (1993b) where shifts -0.011 and -0.15 in  $\log T_e$  and  $M_V$  respectively were required. If a similar  $M_V$  shift applies to Lance's remote population I A stars they would only be at 93% of their indicated distances and  $\log \nu$  would go up with about 0.1 so the quality of the remote tail is not altered. Lance's SGP A stars are fitted by two exponentials with scale heights 121 pc and 1000 – 1600 pc respectively and we note the difference to our sample between 900 and 1300 pc. For a further discussion see Sect. 10.

### 4. The number density – $z(\text{pc})$ variation for A3 – A9 stars

In Fig. 2 was shown the number density data in a 75 pc binning, triangles. As mentioned above we are only volume complete to  $\sim 450$  pc in the sense that the coolest and least luminous A stars would have been included if present. We tried to fit the data within  $\sim 250$  pc with one exponential and those between 450 and 1300 pc with another. The dotted curves in Fig. 2 depict these exponentials with scale heights 65 and 165 pc respectively. The dash dot curve is their sum and was found to represent the data reasonably well on a logarithmic scale but note that the data at 185 pc is more than 40% lower than the fit by two exponentials and that the point at 330 pc is  $\sim 20\%$  above the fit, in later Sects. (6.2 and 6.3) we try to match these deviations and we discuss the significance of such residuals. The most distant point represents a star detected at 1300 pc. The relative occurrence of this two "populations" is 1.00:0.03 in the plane and they carry equal weight at 400 pc, but these scalings may mean nothing, due to the possible incompleteness beyond  $\approx 450$  pc. But why exponentials? There is no simple a priori form of a density law required by the disk's dynamics. A selfgravitating isothermal disk would require a  $\text{sech}^2$  law, van der Kruit (1988), which would be approximated by a gaussian for  $z \sim 0$  pc and by an exponential for  $z$  exceeding a few scaleheights. We think that the data density of the present sample may justify further scrutiny.

Since there is no physical argument to prefer an exponential variation the data might equally well be represented by gaussians and we have consequently adapted a sum of three gaussians, the division 50 – 250 pc 450 – 1300 pc that worked well

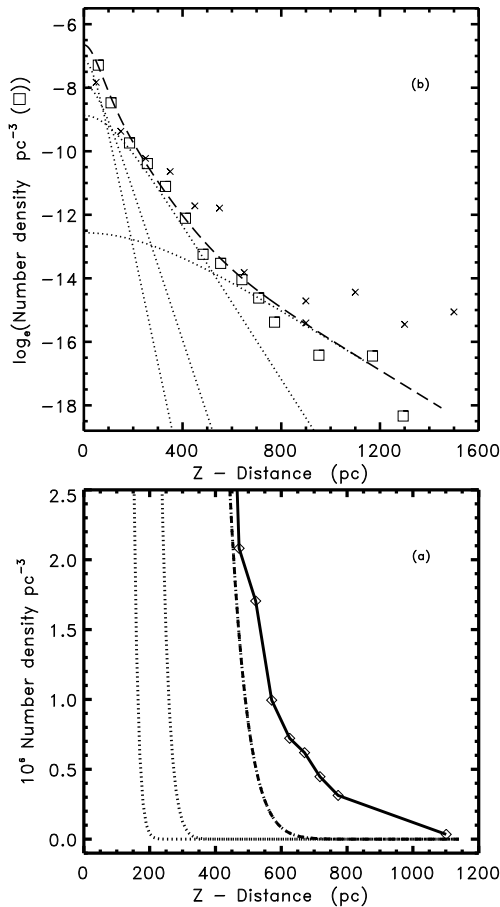


**Fig. 3.** **a.** Number density, not the log, versus  $z$ (pc). Solid curve data. Dashed dotted curve sum of three gaussians indicated with scale heights 45, 75 and 155 pc and relative normalizations 1.0:0.5:0.2 for  $z = 0$  pc 50 pc independent bins. The  $h = 155$  pc gaussian is hidden in the sum. **b.**  $\ln(\text{density})$  ( $\square$ ). Lance density ( $\times$ ). Dotted curves are  $\text{sech}^2(\frac{z}{h})$  with  $h$  equal to 55, 85, 165 and 420 pc respectively. The dashed curve is there sum, 75 pc independent binning

for the exponentials does not work for the gaussians. The range 50 – 250 seems to require more than one component. An additional gaussian with scale height 75 pc is included. For the range 250 – 450 a gaussian with  $h = 155$  pc is implied. At  $z = 0$  the relative normalization of the three gaussians is 1.0:0.5:0.2, Fig. 3. The binning for the gaussian approximation is 50 pc. Between 50 and 450 pc there is a palpable agreement, assuring since it is the  $z$  range where we have volume completeness. Interestingly something similar to the Perry (1969) population with scale height  $\sim 45$  pc is dominating within 100 pc but it was not apparent in the exponential fit. For distances larger than 150 there are most stars from the  $h = 155$  pc population. At 154 pc we find twice as many stars from the  $h = 155$  pc as from the  $h = 75$  pc population.

The gaussian estimate for  $\nu_0$  is, however, vastly too large. For the larger  $z$  values we meet the adverse problem since here the gaussian sum underestimates the observations, Fig. 3a. In Fig. 3a we only show the number density range pertaining to the most distant bins because we want to show it on a linear

scale illustrating the disparity of fit and observations, including the whole density range and maintaining the linear scale would make the fit beyond 450 pc look perfect, from  $z = 0$  to 1300 pc the number density drops with  $\sim 4$  orders of magnitude. The gaussian with  $h = 155$  pc is hidden in the dash - dot curve representing the sum. From about 500 pc the sum of three gaussians underrepresents the observations to a noticeable degree – but not as dramatic as is the case for Lance’s SGP sample.

The situation is such that the curve fitting most of the volume complete distance range underestimates the density beyond the completeness limit! We could of course introduce more gaussians but have chosen to switch  $\text{sech}^2$ s instead, of course guided by scale heights and relative normalizations revealed by the number density discussion. The relevance of gaussians fits are reconsidered in Sect. 8 in another context.

A  $\text{sech}^2(\frac{z}{h})$  law might be a good choice since it has a more pronounced wing than  $\exp(-\frac{z^2}{2h^2})$  for the same  $z = 0$  normalization and we are in need of a contribution beyond  $\sim 500$  pc without enhancing  $\nu_0$ . Our experience from the gaussian sums inspired components with  $h = 55, 85$  and 165 pc. The last 4 – 6 bins,  $z$  from  $\sim 600$  to 1300 pc, seem to follow a  $\text{sech}^2(\frac{z}{420})$  distribution. The sum of these four density laws and a relative normalization 1.00:0.47:0.18:0.005 at  $z = 0$  gives a very good adaption to the density data as Fig. 3b may depict. See however the error discussion in Sect. 6.3. It is important to notice that although we try to match the remote stars the main issue is to adopt a curve to the data within 450 pc. The  $h = 420$  pc component is not completely negligible within our completeness limit of  $\sim 450$  pc, it contributes  $\sim \frac{1}{3}$  at 450 pc and  $\sim \frac{1}{4}$  at  $\sim 400$  pc. We suggest the following sum to represent the density variation for A stars, within 450 pc adapted to a volume complete sample, beyond 450 pc it must necessarily only be taken as a lower limit to the A star density

$$\begin{aligned} \nu(z) = & (1.0000 \text{sech}^2 \frac{z}{55} + 0.4668 \text{sech}^2 \frac{z}{85} \\ & + 0.1790 \text{sech}^2 \frac{z}{165} + 0.0045 \text{sech}^2 \frac{z}{420}) \quad (1) \\ & \times 7.8672 \cdot 10^{-4} \text{pc}^{-3} \end{aligned}$$

Within 450 pc  $\nu(z)$  converts to  $\rho(z)$  by multiplying with the constant mean mass  $\overline{\mathcal{M}}_* = 1.74 \pm 0.03 \mathcal{M}_\odot$ .

Recall that what we term A stars only include A3 – A9. Regarding the numerical constant  $1.74 \times 7.8672 \cdot 10^{-4} = 13.6890 \cdot 10^{-4} \mathcal{M}_\odot \text{pc}^{-3}$  there are two coincidences, perhaps of some interest. First one is that it exactly matches the mass density in the plane of our median star ( $M_V = 2.31$ ,  $\mathcal{M} = 1.73 \mathcal{M}_\odot$ ) which according to Allen (1973) is  $13.84 \cdot 10^{-4} \mathcal{M}_\odot \text{pc}^{-3}$ . Second the sum of four  $\text{sech}^2$  predicts a mass density for our A stars at  $z = 0$  equal to  $(1.0000 + 0.4668 + 0.1790 + 0.0045) 13.6890 \cdot 10^{-4} \mathcal{M}_\odot \text{pc}^{-3} = 22.591 \cdot 10^{-4} \mathcal{M}_\odot \text{pc}^{-3}$ . Adopting the mass fraction 0.021 for stars with  $M_V < 2.5$ , Bahcall (1984b) Table 1, a total identified mass density of  $0.108 \mathcal{M}_\odot \text{pc}^{-3}$  is implied, almost like the observed value.

## 5. Kinematics

Since  $\nu(z)$  is not reproduced by a single function but requires a compound of four  $\text{sech}^2$ , formally isothermal populations, we

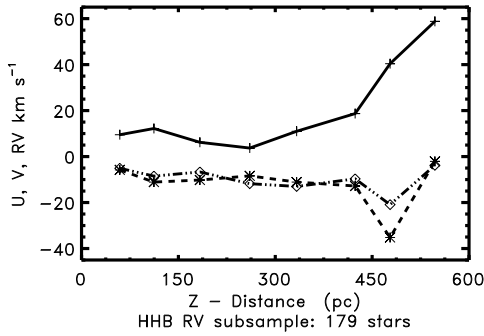


**Fig. 4.** Average U, V and RV velocities of the 179 stars common to Hill et al. (1988). U: solid, V: dashed, RV: dash – dots. U, V and all distances from the present work, RV from Hill et al. (1988). Particularly U shows some variation but V also indicates some shearing, see further discussion in Sect. 6.2.2. RV marginally decreases from  $\sim -5$  to  $\sim -10$   $\text{km s}^{-1}$  at  $\sim 400$  pc

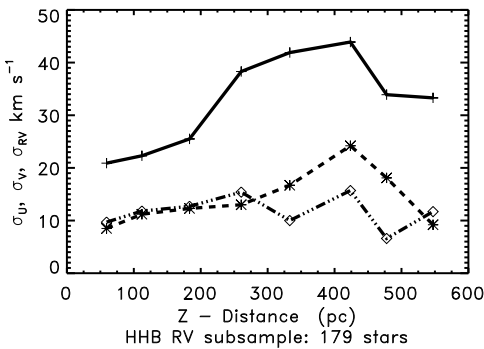


**Fig. 5.** Velocity dispersions based on the 179 stars common to Hill et al. (1988),  $\sigma_U$  and  $\sigma_V$  and distances from the present work  $\sigma_{RV}$  from Hill et al. (1988) RV data.  $\sigma_U$ : solid,  $\sigma_V$ : dashed,  $\sigma_{RV}$ : dash – dots. Apparently the A disk is not quite isothermal

do not anticipate the complete A star population to be isothermal but rather that the RV dispersion should increase with  $z(\text{pc})$  because the scale height of the four components range from 55 to 420 pc and if relaxed these components would imply an increasing  $\sigma_{RV}$ . Ages range from  $< 100 \cdot 10^6$  to about  $1.6 \cdot 10^9$  yr with a median  $7.5 \cdot 10^8$  yr so it may be hard to accept that there exist that old, unmixed components. Still what we observe could formally be represented as a combination of isothermal components in accordance with Gilden and Bahcall’s (1985) statement “...that there be some isothermal that produce a reasonable good fit”.

The A stars all have measured proper motions. 40% of the entries in the photometric catalog was in the AGK3 and their proper motions were taken from the PPM, Röser and Bastian (1993). The remaining 60% was included in the CAMC observing programme from La Palma and may be found in Carlsberg Meridian Catalogue 4 – 8 (1989 – 1994). Particularly the latter are very accurate since they are based on an Astrografic Catalogue – CAMC comparison, with a time base of  $\sim 100$  years. The accuracy is a few m.a.s./yr in  $\mu_\alpha \cos \delta$  and  $\mu_\delta$  implying an uncertainty of  $3 - 4 \text{ km s}^{-1}$  in U and V at the median distance of 230 pc. At 420 pc the proper motion accuracy could mean

that we should apply a rms reduction in  $\sigma_U$  from 38 to 34  $\text{km s}^{-1}$ , which hardly is significant. At the large galactic latitudes approximate U and V values are available for all stars even without RV, the projection only introducing a minor error. Radial velocities are available for 179 of the stars, Hill et al. (1988) – HHB, all above  $b = 75^\circ$ . Fig. 4 and 5 show  $z$  versus U, V, RV and  $\sigma_U, \sigma_V, \sigma_{RV}$  for these 179 stars in independent distance bins. U and V from the present work do not include RV even when available in order to retain a sample treated systematically. U shows a dramatic increase beyond 300 pc, from about 10  $\text{km s}^{-1}$  to more than 50  $\text{km s}^{-1}$ . From 50 to 450 pc both V and RV decreases from around  $-5 \text{ km s}^{-1}$  to around  $-10 \text{ km s}^{-1}$ . More importantly we might see the dispersions increase with  $z(\text{pc})$  – an increase that could be caused by increasing influence from groups of stars with increasingly larger scale heights. For a further discussion of the variation of the velocity dispersions with distance see Sect. 9 and 10 though.  $\sigma_U$  and  $\sigma_V$  both go up with a factor 2.5 over the range from 50 to 450 pc.  $\sigma_{RV}$  may increase with about 50% over the range from 50 to 300 pc as does  $\sigma_U$ . Since the RV sample is not volume complete the  $z - \sigma_{RV}$  evaluation is necessarily less certain than the  $z - \sigma_U$  discussion. The more remote stars appear to carry more kinetic energy than those closer to the galactic plane. Since the four formal A star “populations” resulting from the fit to the data of course see the same total disk density and the same potential the ratio  $\sigma_{RV}^2/h^2$  should be constant for any relaxed component well within  $\approx 200$  pc, Bahcall (1984a, 1984b), Gilden and Bahcall (1985). This could in fact be the case since we see scale height variations of the order of 2 to 3 and variations of the same order for the velocity dispersions. According to Fig. 5  $\sigma_{RV}$  might flatten out beyond 300 pc, at least there is no clear increase, rather a noisy behaviour instead. At distances beyond a few hundred pc the HHB sample could be dominated by only one isothermal population with  $\sigma_{RV} \gtrsim 15 \text{ km s}^{-1}$ . A few hundred more radial velocities would be nice to have, if possible for the stars in the  $z(\text{pc})$  range 200 – 1300 pc.

Finally we show in Fig. 6a the run of  $\sigma_U$  for the entire sample.  $\sigma_U \approx 50 \text{ km s}^{-1}$  at the completeness limit.  $\sigma_U$  reaches  $\approx 70 \text{ km s}^{-1}$  at 1 kpc. If the most remote bin was extended to include the star at 1300 pc the final drop would not take place. If the standard relaxed ratio between  $\sigma_U$  and  $\sigma_W$  is maintained in the polar region  $\sigma_W$  would be around  $30 - 40 \text{ km s}^{-1}$  for the stars more distant than 800 pc a large number but not quite the  $66 \text{ km s}^{-1}$  found by Lance (1988). Within 450 pc each bin contains  $\gtrsim 30$  stars. Fig. 6a also contains the run of  $\sigma_U$  with subgiants excluded.

The U distribution for the complete sample may not be fitted by a single gaussian. A reasonable fit is obtained from three gaussians with dispersions 25.5, 17.5 and  $33.0 \text{ km s}^{-1}$ , and mean values  $-8.0, 1.0$  and  $11.2 \text{ km s}^{-1}$  and relative normalizations 1.0:3.1:6.2, the U dispersion of the complete set of A stars is  $33.0 \text{ km s}^{-1}$ . The kurtosis also imply that U does not obey a gaussian distribution. The U distribution from the 100 pc bins we are introducing in Sect. 6 may apparently be fitted by single gaussians. Fig. 6c is an example of this. For later use Fig. 6d displays that the age distribution may be peculiar. The 115 – 215

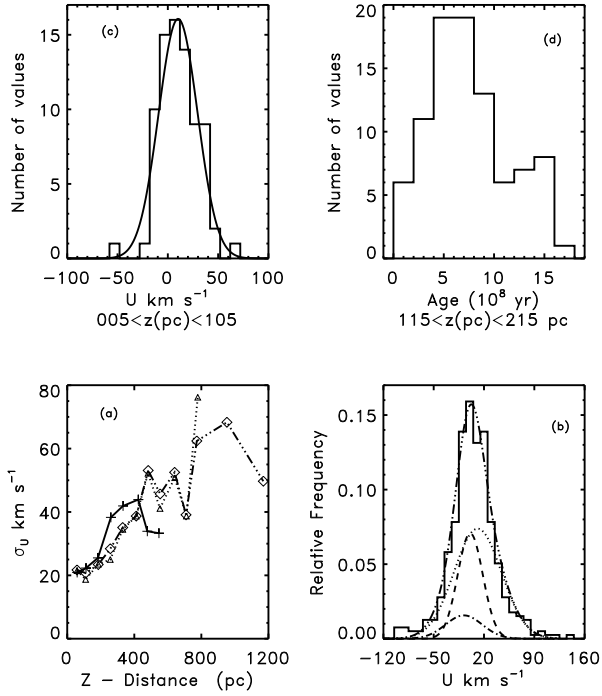


**Fig. 6.** **a.** 75 pc independent distance bins. U dispersions based on the 396 stars above  $70^\circ$  compared to the dispersion from stars common to Hill et al. (1988) exclusively.  $\sigma_U$  (HHB – subsample): solid,  $\sigma_U$  (complete sample): dash – dots. The A disk is seen not to be isothermal with  $\sigma_U$  apparently increasing from  $\sim 20$  to  $\sim 70$   $\text{km s}^{-1}$ . Recall that sample is not volume complete beyond 450 pc. The dashed curve depicts the U dispersion excluding the A subgiants,  $\delta c_0 > 0.150$ . **b.** Distribution of 396 U velocities and the fit by three Gaussians with different mean and dispersion. **c.** U distribution for stars between 30 and 105 pc, both age groups, fitted by a single Gaussian with mean 10.2 and dispersion 19.4  $\text{km s}^{-1}$ . **d.** Age distribution for stars between 115 and 215 pc

pc bin is dominated by stars that are younger than the sample median 0.75 Gyr, this may be an example of a distance bin with an age spread implying various degrees of relaxation.

For a more detailed discussion of the kinematics see Sects. 6, 7 and 10, Fig. 17, but we may probably already conclude this section by stating that the set of A stars does not form an isothermal group of stars.

## 6. Density and angular momentum variation within 450 pc

The equation  $\rho_{total}(z=0) = (2\pi G)^{-1} z^{-2} \sigma_W^2 \ln[\frac{\rho_k(0)}{\rho_k(z)}]$ , Eq. (5) from Bahcall (1984b) estimates the total disk density from the density variation of an isothermal tracer  $k$  near the plane. With a Gaussian variation  $\rho_{total}(z=0) \propto [\frac{\sigma_W}{h}]^2 \sim \text{constant}$ . Gildden and Bahcall (1985) apply the constancy of  $\frac{\sigma_W}{h}$  as a consistency check of trial potentials.

### 6.1. Independent distance bins

As demonstrated above the A stars'  $z(\text{pc})$  – density distribution may be approximated with a sum of four  $\text{sech}^2(\frac{z}{h})$  populations

**Table 1.** Effective scale heights  $h_{eff}$  and the constancy of the  $\sigma_W/h_{eff}$  ratio. 75 pc independent bins

$z$	$h_{eff}$	$\sigma_W = 0.47 \times \sigma_U$	$\frac{\sigma_W}{h_{eff}}$	$\frac{\sigma_V}{\sigma_U}$
pc	pc	$\text{km s}^{-1}$	$\text{km s}^{-1} \text{pc}^{-1}$	-
55	88.22	9.94	0.1127	0.52
85	102.70	10.89	0.1060	0.59
165	151.14	11.83	0.0783	0.57
420	177.62	19.80	0.1118	0.44

possibly indicating a variation that is a sum of isothermal distributions who do not, however, sum to an isothermal. Since half our sample has  $RV \approx W$  velocities and the sample has U and V velocities we may investigate the ratio  $\sigma_W/\sigma_U$  variation with  $z$ . We bin the HHB subsample in 75 pc bins and confine  $z$  to be within 375 pc for completeness reasons, see Fig. 5 and Fig. 6a. Including the four first distance slots  $\sigma_W/\sigma_U = 0.47 \pm 0.05$  and with five distance bins  $\sigma_W/\sigma_U = 0.43 \pm 0.11$ . Since the A stars are younger than  $\sim 1.5$  Gyr we might compare the  $\sigma_W/\sigma_U$  ratio to that from equally young F stars. Marsakov and Shevelev (1994) find  $\sigma_W/\sigma_U$  in the range 0.4 – 0.5 for F stars younger than 2 Gyr somewhat dependent on metallicity though. Palouš and Piskunov (1985) did a study of the temporal evolution of bright B and A stars motion. They estimate the time required for relaxing the velocity ellipsoid to  $2 \cdot 10^8$  yr after which the ratio  $\sigma_W/\sigma_U = 0.47 \pm 0.08$ . 31 stars or 8% of our sample are younger than  $2 \cdot 10^8$  yr. So our own estimate 0.47 – 0.43 may apparently be used with a slight preference for the value 0.47. But as may become evident later such a short relaxation time may be challenged by the NGP A stars.

At any distance within 450 pc the measured  $\sigma_U$ ,  $\sigma_V$  dispersions are a result of the actual stellar mixture at that distance. At larger distances we have much fewer stars and may bias our dispersions if there is a luminosity – velocity relationship caused by the limiting magnitude. The following discussion is confined to the volume within 450 pc. As mentioned the measurements of stars at a given distance provide the true velocity mixture but what is the corresponding scale height? We are not able to assign the population membership of individual stars but at each distance we may compute the weighted scale height from the proposed  $z - \nu(z)$  law given in Sect. 4 in the sense that we know which fraction each of the four  $\text{sech}^2$  contributes.  $\sigma_W$  is computed from  $\sigma_U$  (complete sample) at the same distance and the constant  $\sigma_W/\sigma_U$  ratio 0.43 – 0.47.

Table 1 presents the resulting effective scale heights,  $h_{eff}$ , the computed dispersion  $\sigma_W$  and the ratio  $\sigma_W/h_{eff}$ . We need not use the computed W dispersion but might as well use the values measured for about half the sample the value at 420 pc is an extrapolation though. Interestingly Perry (1969) measures  $\sigma_W = 18.4$   $\text{km s}^{-1}$  for his sample of A0 – A2 stars. We have chosen the four formal scale heights as test distances. Column 2 of Table 1 give the resulting effective scale heights. Interesting to note the rather small effective scale height of only 177.6 pc for

the stars at 420 pc. The resulting ratios at the four test distances has an average  $\langle \frac{\sigma_W}{h_{eff}} \rangle = 0.100 \pm 0.015$ , the ratio may be considered virtually constant. Excluding the  $z = 420$  pc point  $\langle \frac{\sigma_W}{h_{eff}} \rangle = 0.099 \pm 0.018$ . The value at 165 pc deviates. A discussion of this discrepancy is offered in Sect. 6.2. The last of Table 1's columns displays  $\sigma_V/\sigma_U$  ratio. The first three entries do not show much variation, this may be misleading, see Fig. 15c.

At this point we might have the impression that since  $\frac{\sigma_V}{\sigma_U}$  and  $\frac{\sigma_W}{h_{eff}}$  approximates their canonical relaxed values and  $\frac{\sigma_W}{h_{eff}}$  seems constant the combined density and velocity data meets the assumptions underlying Jeans' equation. The concomitant increase of  $\sigma_W$  and  $h_{eff}$  apparently mimics the behaviour of a steady state tracer. But the deviation of  $\frac{\sigma_W}{h_{eff}}$  at 165 pc should be investigated further.

## 6.2. Running 100 pc bins

The computation of different values for  $\frac{\sigma_W}{h_{eff}}$  at  $z$  equal to 55 and 85 and at  $z = 165$  pc respectively and the residuals mentioned in Sect. 4 have prompted a further investigation of the variation of densities and kinematics.

So far we have used discrepant distance intervals which may cause peculiarities in the computed density and velocity dispersions if some irregularities occur. Or conversely may overlook fluctuations if the reference distances are not suitably chosen. As a remedy we compute mean distance, density and velocity means and dispersions for intervals centered at each integer  $z$  including all stars between  $z-50$  and  $z+50$  pc; if  $z-50 < 0$  the volume is computed from 0 to  $z+50$ . The nearest star is at 30 pc but changing 0 to 30 pc will only alter the nearest volume with  $\approx 2\%$ . We did the same exercise for  $z-37.5$ ,  $z+37.5$  bins but the resulting  $z$  variation of density and kinematic parameters did not show any significant quantitative changes. Fig. 7a shows the number density distribution with height for the running 100 pc bins. Densities from the 75 pc independent bins are also included (filled circles) and are seen to match the running 100 pc means nicely and thus follow the general trend of the density curve from the running bins. Compared to Fig. 3b Fig. 7a elucidates some details, e.g. a hump (or a ledge) between 150 and 300 pc not so evident with Fig. 3b's binning. The distribution has a rather clear ledge protruding from  $\sim 150$  pc. This is interesting since 150 is close to 165 pc where we computed the smallest  $\frac{\sigma_W}{h_{eff}}$  ratio. We recall that the sample includes all A stars within  $\sim 450$  pc and the hottest ones within  $\sim 675$  pc so there should be no sampling problems at 150 pc, see Fig. 16a though. Why not use the fit from Fig. 3b superposed as the dash dot curve? We notice systematic differences from the observations at  $\sim 170$ ,  $\sim 300$  and  $\sim 430$  pc where Eq. (1) overestimates the density by  $\sim 40\%$ , underestimates by  $\sim 30\%$  and overestimates by  $\sim 30\%$  respectively. The significance of these deviations is discussed in Sect. 6.3. On the other hand the correspondence between the independent densities and the estimate from the running bins is better than 10%. As discussed below the uncertainty of the independent density estimates is better than 10% except for the bin 375 – 450 pc where it is 15%. The agreement between the

densities from the 75 pc independent bins and the running bins indicates that the correlation of neighboring points in the running mean does not introduce artificial sampling features. The deviations of 40, 30 and 30% at 170, 300 and 430 pc correspond to  $\sim 35$ ,  $\sim 25$  and  $\sim 10$  stars respectively in the 100 pc bins. The fit ought to be improved to remove such residuals. We try to match the ‘‘continuous’’ observations with a sum of sech squared but fails to reproduce the humpy region. The thin solid curve represents the sum of the three sech<sup>2</sup>s required to fit the data between 50 and 150 pc. If we limit ourselves to the use of sech<sup>2</sup>s in the curve fitting the only way the observations may be reproduced is by introducing two components showing density maxima away from the plane, at 200 and 250 pc respectively and with scale lengths 30 and 100 pc respectively. With the discrepant 75 pc binning the largest scale height required was 415 pc. The running 100 pc binning may only be fitted within the completeness limit 450 pc, if a sech squared with scale height 680 pc is added. The data nearest to the plane is taken care of by two groups with scale heights 75 and 175 pc. The complete curve is fitted by a sum of five sech squared, two of which are not peaking for  $z=0$ . The 100 pc running density thus alters our fit by introducing a large scale height 680 pc and two components concentrated some hundred pc above the plane. The dashed curve of Fig. 7a shows the almost perfect fit out till 675 pc and we note that a part from sech<sup>2</sup>( $\frac{z}{680}$ ) the remaining four components have identical densities at  $\sim 200$  pc. We perform the same procedure for stars younger than the median 0.75 Gyr, the scale heights 75 and 175 are changed marginally to 85 and 185 pc. And the sech<sup>2</sup> peaking at 250 pc now has a scale length of 80 pc instead of 100 pc. The problem with the young stars is the  $z$  range from 400 to 450 pc. The inclusion of any large scale height component causes an overestimate of the density within 400 pc. The range 400 – 450 pc may be included in the fit by adding a sech<sup>2</sup> centered at 475 with scale height 40 pc. Fig. 7b shows the final fit and the compounded curve follows the data for the stars younger than the median well within 450 pc. As discussed in Sect. 9 young stars are less frequent beyond  $\sim 200$  pc or rather they are overabundant nearest to the plane. There is one discrepancy at  $\approx 75$  pc, probably caused by A stars related to the Coma cluster at 80 pc. Finally we show the fit to the density variation for stars older than 0.75 Gyr in Fig. 7c.  $7.5 \cdot 10^8$  yr is chosen for two reasons. It is the sample median age and is close to the age of the Hyades. Fig. 6d gives evidence on the age distribution for the stars between 115 and 215 pc, a distance slot we know to be interesting by providing a discrepant  $\frac{\sigma_W}{h_{eff}}$  estimate. In the fit of Fig. 7c we have not included the component centered on  $z = 200$  pc in the sum to show its relative significance. The old stars alone require the  $h = 680$  pc component for the fit within 450 pc, by chance this component also fits the data beyond 450. The sum of the four components is only shown within 450 pc.

The change to running intervals thus suggests the presence of an old, A: 0.75 – 1.5 Gyr, large scale height, 680 pc, population and the possibility to have minor formal components peaking at  $z \gg 0$  pc.

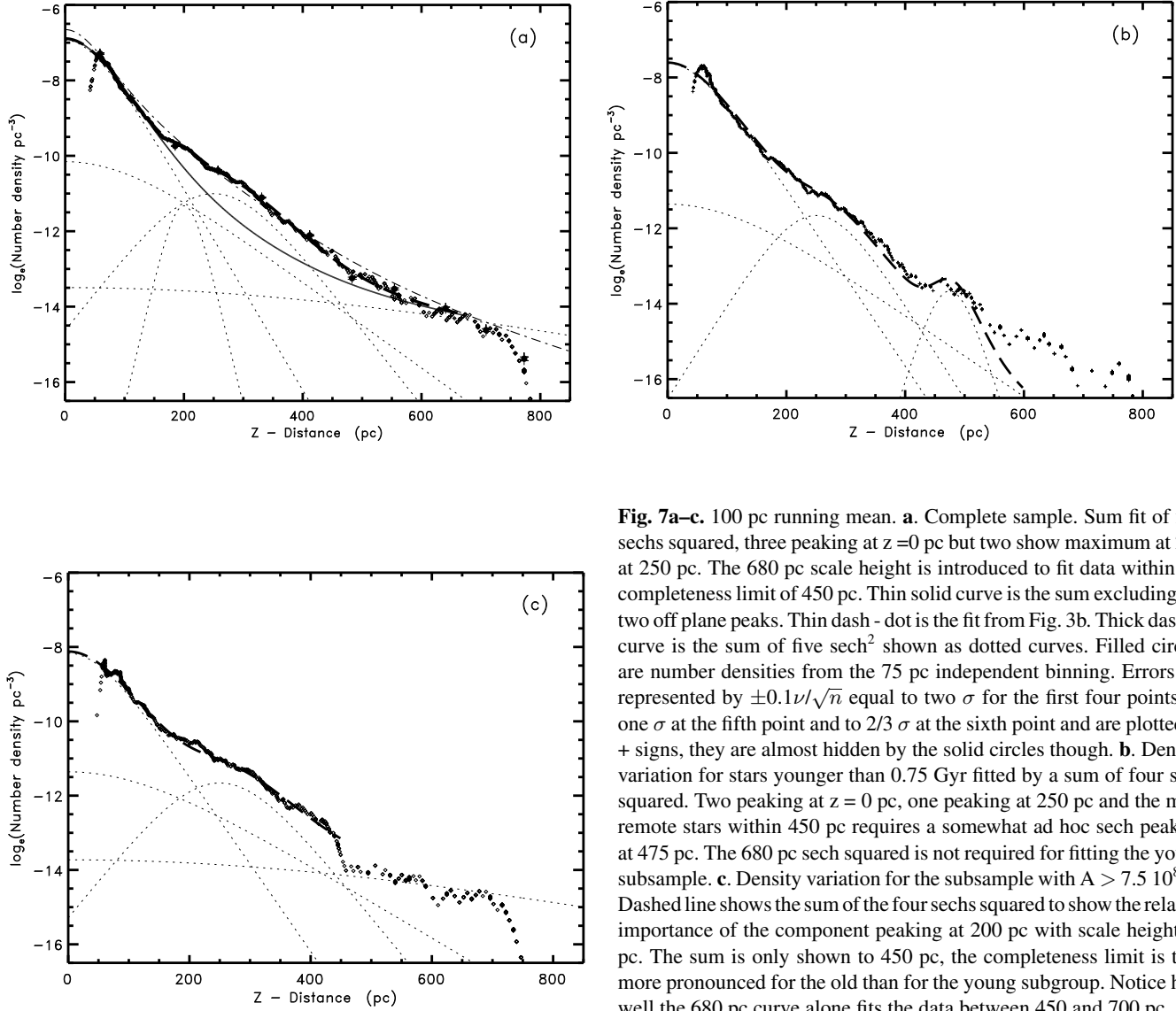


**Fig. 7a–c.** 100 pc running mean. **a.** Complete sample. Sum fit of five sech<sup>2</sup>s, three peaking at  $z=0$  pc but two show maximum at 200 at 250 pc. The 680 pc scale height is introduced to fit data within the completeness limit of 450 pc. Thin solid curve is the sum excluding the two off plane peaks. Thin dash-dot is the fit from Fig. 3b. Thick dashed curve is the sum of five sech<sup>2</sup> shown as dotted curves. Filled circles are number densities from the 75 pc independent binning. Errors are represented by  $\pm 0.1\nu/\sqrt{n}$  equal to two  $\sigma$  for the first four points, to one  $\sigma$  at the fifth point and to  $2/3 \sigma$  at the sixth point and are plotted as + signs, they are almost hidden by the solid circles though. **b.** Density variation for stars younger than 0.75 Gyr fitted by a sum of four sech squared. Two peaking at  $z=0$  pc, one peaking at 250 pc and the most remote stars within 450 pc requires a somewhat ad hoc sech peaking at 475 pc. The 680 pc sech squared is not required for fitting the young subsample. **c.** Density variation for the subsample with  $A > 7.5 \cdot 10^8$  yr. Dashed line shows the sum of the four sech squared to show the relative importance of the component peaking at 200 pc with scale height 30 pc. The sum is only shown to 450 pc, the completeness limit is thus more pronounced for the old than for the young subgroup. Notice how well the 680 pc curve alone fits the data between 450 and 700 pc

The philosophy behind the fit in Fig. 7a is to match the observations better than Fig. 3b even if this means the introduction of curves peaking off the plane but with as few curves as possible. The combined curve resulting from the detailed match allows differentiation which elucidates the nature of the  $z$  variation, See Sect. 8.

### 6.3. Errors in density fits and in density data

From the error progression in the fit by sums of  $\nu_0 \operatorname{sech}^2(\frac{z}{h_i})$ s we compute  $\frac{\sigma_\nu}{\nu} = (\sum (\frac{\sigma_{\nu_0}}{\nu_0})^2 + \sum 4w_i \tanh^2(\frac{z}{h_i})(\frac{z}{h_i})^2)^{1/2}$  assuming errors in  $(\nu_0)_i$  and scale height  $h_i$  only. Weights  $w_i$  are adopted from the fit presented in Fig. 3b and Eq. (1). The formula is based on the assumption that  $\sigma_{h_i} = 0.2h_i$ .  $\sum (\frac{\sigma_{\nu_0}}{\nu_0})^2$  is estimated from the different estimates in Fig. 3b and Fig. 7a. The computation of  $\frac{\sigma_\nu}{\nu}$  shows that  $\sum (\frac{\sigma_{\nu_0}}{\nu_0})^2$  dominates at all  $z$  between 50 and 450 pc. This means that the uncertainty in the fit is  $\pm 0.1\nu(z)$  at any  $z$  and mainly is caused by the uncertainty in  $\nu_0$ . Since the residuals

at 170, 300 and 430 pc exceeds the uncertainty in the sum of four sech<sup>2</sup>s by  $\gtrsim 3\sigma$  there is good reason to attempt a better approximation.

In a similar way the standard error in the observed density  $\nu = n(V)/V \text{ pc}^{-3}$  may be estimated.  $V$  is the volume between the two confining distances  $h_l$  and  $h_u = h_l + \Delta$ .  $\Delta$  is kept constant so  $V = 3\Delta h_l^2 + 3\Delta^2 h_l + \Delta^3$ .  $\sigma_\nu^2 = (\frac{\partial \nu}{\partial h_l})^2 \sigma_{h_l}^2 + (\frac{\partial \nu}{\partial n})^2 \sigma_n^2$ . We assume  $\sigma_{h_l} = 0.15h_l$  as for an individual A star distance. If  $\sigma_n^2 = n$ ,  $\sigma_\nu^2$  reduces to  $\frac{\nu^2}{n} (1 + 0.15^2 (\frac{\pi}{3} \tan^2 20)^2 (6\Delta h_l + 3\Delta^2 \frac{\nu}{n}))$  with  $\Delta = 75$  pc (or 100 pc) the second term is negligible, for  $\Delta = 75$  pc it is a factor  $10^{-3}$  less than 1. So  $\sigma_\nu \approx \frac{\nu}{\sqrt{n}}$ . For most of the intervals  $\sigma_n^2 = n$  seems an overestimate. Since we know the relative error of the individual stellar distances we may calculate the probability to be outside the counting volume for each star. At the distances confining the independent intervals we may compute the migration across, out of and into the interval. Summing the migration across the two boundaries

gives an estimate of  $\sigma_n$  for each independent bin. We could also use the rms of  $n_{in}$  and  $n_{out}$  but apart from the interval 300 – 375 pc where the two estimates are 1 and 6 respectively the two estimates do not differ. For all intervals  $\sigma_n < \sqrt{n}$ . Within  $z = 300$  pc and  $\Delta = 75$  pc  $\sigma_n < 0.05n$ ,  $0.09n$  between 300 and 375 pc and  $0.14n$  for the 375 – 450 pc bin, the latter is an overestimate though since too few stars are scattered in from 450 – 525 pc due to the volume incompleteness beyond 450 pc.

At  $\sim 170$  pc where the fit in Fig. 3b differs  $\sim 40\%$  from the data we may calculate  $(\frac{\sigma_v}{v})^2 = (\frac{\sigma_v}{v})_{fitFig. 3b}^2 + (\frac{\sigma_v}{v})_{data}^2 = 0.1^2 + 0.05^2$  implying  $\frac{\sigma_v}{v} = 0.11$  less than 0.40 a similar significance is found at  $\sim 300$  pc but at 430 pc  $\frac{\sigma_v}{v} = 0.35$  making the difference between the fit of Fig. 3b and the data, 0.30, insignificant. The distance  $\sim 170$  pc is particularly important since it is where the ledge starts protruding.

The ledge at 150 pc in Fig. 7a deserves a comment: According to Gildea and Bahcall (1985) density profiles that have plateaus should be rejected in the isothermal context. But as we hesitate to abandon the data perhaps the isothermal assumption has to be reconsidered for the A stars.

#### 6.4. Kinematics versus distance

The clearest evidence of kinematic peculiarities at  $\sim 200$  and  $\sim 250$  pc is probably given by the variation of the angular momentum with  $z$ . The angular momentum is computed assuming a distance of 8.5 kpc to the galactic center. The young, old and combined sample show peculiarities in the momentum at  $\sim 250$  pc. In Fig. 8a is shown the momentum –  $z$  variation for the young subsample and we notice the change of slope at 150 pc. In Fig. 8b we have the variation for the total sample of A stars and again we see the depression at 150 pc. At 250 pc the momentum has a local extremum matching the mean  $z$  value of the most prominent off plane group required to fit the density variation for all stars in Fig. 7a. Fig. 8b indicates an apparent decrease of the angular momentum between 50 and 150 pc where a rise in the angular momentum sets in. This means that 100 pc bins centered at distances larger than  $\sim 100$  pc include stars from a range where the kinematics may be slightly peculiar by having lower  $\sigma_U$  and larger angular momentum. The filled circles in Fig. 8b again represent values from the 75 pc independent binning with mean errors indicated. The values between 100 and 200 pc are smaller than the momentum at 50 and 250 pc on the  $2\sigma$  level.

Unfortunately  $\sigma_W$  is not available for the complete sample so the pressure  $\nu(\sigma_U^2 + \sigma_V^2 + \sigma_W^2)$  may not be computed in a consistent way but in Fig. 8c we display our best approximation of the A stars' capacity to resist the Galaxy's gravitational pull including the rotational support, beyond  $\sim 150$  pc the A stars show an increased energy density and we notice the small humps at  $\sim 200$  and  $\sim 250$  pc. The energy density of the HHB RV subsample (crosses), including  $\sigma_W^2$ , shows a similar tendency to follow two exponentials but the shift to the more shallow one takes place at  $\sim 250$  pc.

We may conclude that the distance of the main off plane density peak coincides with the location of enhanced angular

**Table 2.**  $\frac{\sigma_U}{h_{eff}}$  for stars younger than 0.75 Gyr. Effective scale height from fit to density –  $z$  variation including off plane groups

$z$	Number of stars	$\sigma_U$	$h_{eff}$	$\frac{\sigma_U}{h_{eff}}$
pc	–	km s <sup>-1</sup>	pc	km s <sup>-1</sup> pc <sup>-1</sup>
55.0	24	18.8	88.25	0.213
83.4	65	18.2	89.56	0.203
99.9	72	19.3	90.70	0.213
150.1	56	22.0	95.83	0.230
165.1	51	23.6	97.11	0.243

momentum and with depressed U dispersions and with partial energy density  $\nu(\sigma_U^2 + \sigma_V^2 + (V + 220)^2)$  enhancements.

#### 6.5. $\frac{\sigma_U}{h_{eff}}$ for young and old subgroups with 100 pc binning

The average velocity and dispersion are results of the actual stellar mixture and since this mixture, at any distance, is not represented by any pure isothermal component we compute  $h_{eff}$  as the weighted average of the scale heights from the sechs squared reproducing the observed density variation in Fig. 7. The off plane subgroups contribute to this weighted average by replacing the scale height with  $(z_{max} - h)$  where  $z_{max}$  is where the subgroup's number density peaks. The off plane subgroups give rise to an increase of the effective scale height. Very slight due to their small relative frequency. In Table 2 we present the results from the young subsample and in Table 3 those resulting from the old subgroup. A priori the old subsample is expected to represent a larger degree of phase mixing having completed  $\gtrsim 10$  oscillations through the plane and  $\gtrsim 3$  revolutions around the center.

As apparent from Table 2 the effective scale height changes very little, from 88 to 97 pc, when  $z$  is changed from 55 to 165 pc clearly showing how concentrated the young subgroup is towards the plane.  $\sigma_U$  increases by 25%. The ratio  $\langle \frac{\sigma_W}{h_{eff}} \rangle = 0.104 \pm 0.007$ , much like before for the complete sample but with a smaller scatter and no discrepancy at 165 pc as in Table 1.

In Table 3 we show the results from the old subgroup. We notice that  $h_{eff}$  shows a larger range than the young subgroup and that the dispersions generally are larger than the young subgroup's and increase by 35% when  $z$  is raised from 55 to 165 pc. The ratio  $\langle \frac{\sigma_W}{h_{eff}} \rangle = 0.097 \pm 0.009$ , almost as for the young subsample but smaller since the old stars include components with larger scale heights. For similar  $z$  the old subgroup always has a larger effective scale height than the young subgroup. The low computed value of the  $\frac{\sigma_U}{h_{eff}}$  ratio at 150.0 pc is probably caused by peculiar kinematics for the stars centered on 150 pc, see Fig. 8.

Since the two groups defined by the median age show a different behaviour the combined sample may probably not be used as a tracer of density and kinematics. Further consequences of the age variation are discussed in Sects. 9 and 10 but it is

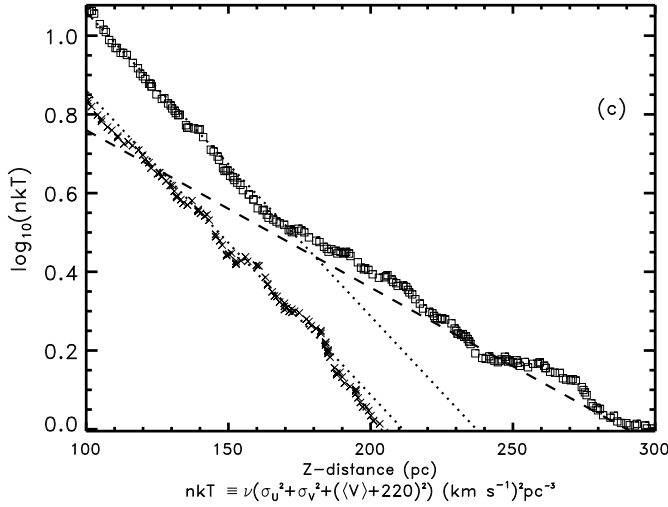
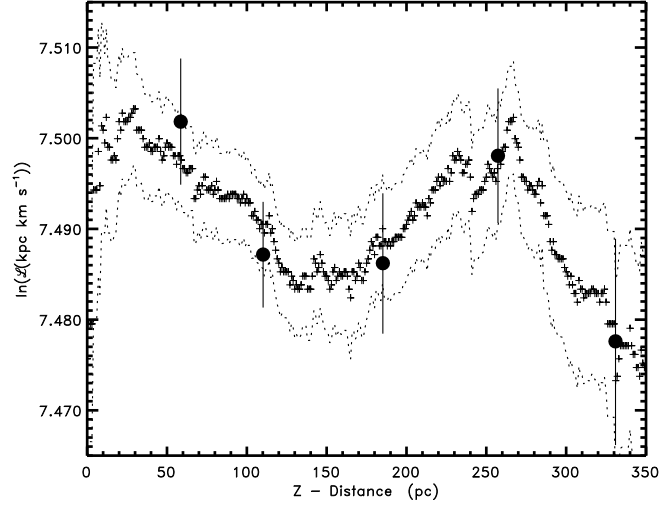
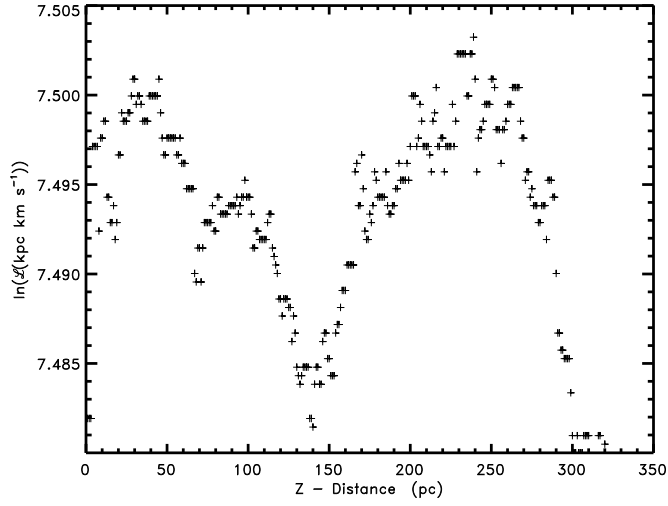


**Fig. 8.** **a** angular momentum for stars younger than  $7.5 \cdot 10^8$  yr. **b** Angular momentum for the complete sample. Dotted curves are mean  $\pm$  error of the mean and the filled circles with errors bars are the values from the 75 pc independent binning. **c**  $nkT \equiv \nu(\sigma_U^2 + \sigma_V^2 + (\langle V \rangle + 220)^2)$  is the sum of a partial pressure and the rotational energy density for the complete A star sample,  $\square$ s. The crosses are for the HHB subsample and since  $\sigma_W^2$  is included  $nkT$  represent the sum of the pressure and the rotational energy density but only for about  $\approx 50\%$  of the sample

**Table 3.**  $\frac{\sigma_U}{h_{eff}}$  for stars older than 0.75 Gyr. Effective scale height from fit to density – z variation including off plane groups

z	Number of stars	$\sigma_U$	$h_{eff}$	$\frac{\sigma_U}{h_{eff}}$
pc	–	km s <sup>-1</sup>	pc	km s <sup>-1</sup> pc <sup>-1</sup>
55.0	6	20.3	94.75	0.214
83.7	33	21.4	99.20	0.215
99.8	48	23.2	103.15	0.225
150.0	43	21.8	124.55	0.175
165.2	46	27.5	133.82	0.205

tentatively suggested that the sample may not be in a steady state.

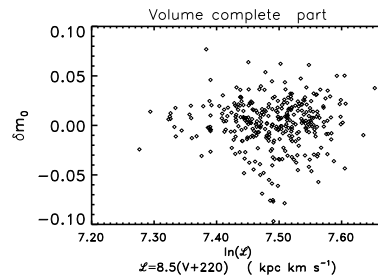


**Fig. 9.** The metallicity parameter  $\delta m_0$  versus angular momentum for stars within 450 pc. Am candidates have  $\delta m_0 < -0.025$

## 7. Can obvious kinematically peculiar groups be identified?

Before we proceed to a discussion of whether the A stars may be used as a tracer of the potential we try to isolate possible contributors to the hump at  $\sim 200 - 250$  pc. We know that the angular momentum and the U dispersion are peculiar at these distances. Stellar metallicity is known to vary with angular mo-

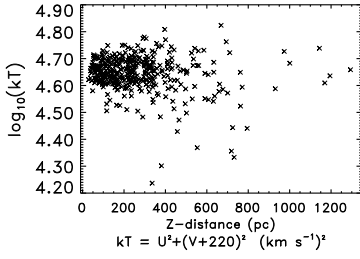


**Fig. 10.** Temperature of the motion parallel to the disk versus distance from the disk

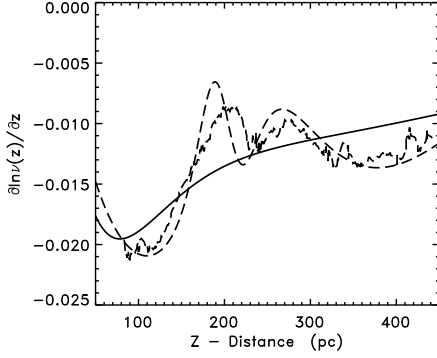


**Fig. 11.** Comparison of derivative of data and of the fitted sum of  $\text{sech}^2$  shown in Fig. 7a. For an isothermal exponential  $\partial \ln \nu(z) / \partial z \propto -1/h$  and for a gaussian to  $-z/h$ . The solid curve is from the sum of four  $\text{sech}^2$  discussed in Sect. 4

mentum. Fig. 9 shows this. The Am stars is seen to occupy a well defined region. Excluding the Am stars does, however, not alter the density variation. According to Fig. 9 the lower left envelope follows the general angular momentum – metallicity trend. The only trend is thus that the Am candidates do not show as low angular momenta as the solar metallicity stars. The sample also contains another homogeneous group with systematically low  $kT \equiv (U^2 + (V+220)^2) (\text{km s}^{-1})^2$  that even concentrates at  $z \approx 200$  pc but contains to few stars to influence the density variation. Fig. 10 further shows that  $kT$  as defined above has a rather narrow range within 450 pc.

### 8. May $4\pi G\rho = -\partial K_z / \partial z$ be used?

For an isothermal tracer of the potential  $\partial \ln \nu(z) / \partial z$  is proportional to  $K_z / \sigma_W^2$  and if  $\nu$  follows an exponential also proportional to  $-h^{-1}$  if  $\nu$  obeys a gaussian the gradient varies proportional to  $-zh^{-1}$ . Fig. 11 displays  $\partial \ln \nu(z) / \partial z$  for the data and for the fit by the sum of five  $\text{sech}^2$ s – including the two peaking off the plane. There is a reasonable correspondence. The figure may give the impression that the sample is comprised by two exponential subsets. One with  $h^{-1} \approx 0.020$  and a second with  $h^{-1} \approx 0.011$  and a transition zone between 130 and 200 pc. There are no indications of any isothermal gaussian. The zero order approximation, isothermality, does accordingly not work.

The solid curve in Fig. 11 is the derivative of the fit formed by four  $\text{sech}^2$ s discussed in Sect. 4, Eq. (1). It is based on independent 75 pc distance bins.  $\partial \ln \nu(z) / \partial z$  seems linear for the

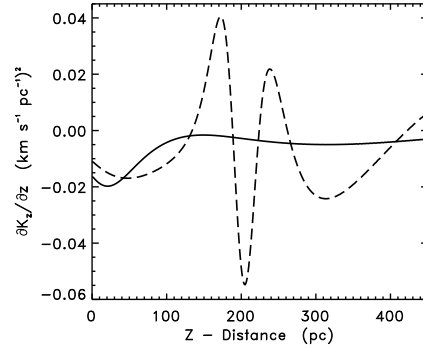


**Fig. 12.** The derivative of Jeans' equation  $\frac{\partial}{\partial z} K_z = -\frac{\partial}{\partial z} \left[ \frac{1}{\nu} \frac{\partial}{\partial z} (\nu \sigma_W^2) \right]$ . For a relaxed tracer near the galactic plane  $\frac{\partial}{\partial z} K_z$  is proportional to the local volume mass density  $4\pi G\rho$ . The solid curve is based on the fit in Eq. (1)

range 100 – 200 pc and for 200 – 450 pc. Is this an indication that the density may be approximated by two gaussians? If so their scale heights become 129 and 250 pc respectively, values not encountered when the use of gaussians were discussed in Sect. 4.  $\sigma_W$  increases from 9.0 to 14.5  $\text{km s}^{-1}$  over the the 100 – 200 pc interval. Not quite constant but if we postulate isothermality and use a gaussian with  $h = 129$  pc at 100, 150 and 200 pc Bahcall's (1984b) approximation returns 0.090, 0.122 and 0.157  $\mathcal{M}_\odot \text{pc}^{-3}$ . A 25% uncertainty is noticed.

Adopting a linear approximation to the  $\sigma_{RV}$  versus  $z(\text{pc})$  variation from the data within 300 pc and an independent binning, see Fig. 5 and Fig. 6a, we may estimate  $\partial K_z / \partial z$  from  $\nu(z)$  and  $\sigma_{RV}$ . This is a very uncertain method due to the several differentiations involved. Bahcall's (1984a, 1984b) method is in fact an attempt to minimize the uncertainties introduced the differentiations.  $K_z$  is from Jeans' equation:  $K_z = -\frac{1}{\nu} \frac{\partial}{\partial z} (\nu(z) \sigma_W^2)$ .  $\partial K_z / \partial z$ , with  $\nu$  replaced by the fitted curve, is shown in Fig. 12. Our linear  $\sigma_{RV} - z$  relation is a first order approximation to the data, we don't assume isothermality. We see that  $\partial K_z / \partial z$  is far from constant, in the range from 50 to 120 pc where  $-\partial K_z / \partial z$  is positive it varies with a factor 2. This factor is the accuracy with which we may calculate  $\rho_{total}$  from the A stars if we postulate that Jeans' and Poisson's equations may be combined. A disappointing result not to be known a priori.

We may again return to the density fit from Eq. (1), mainly leaving out the off plane contributions.  $\partial K_z / \partial z$  from this fit, assuming the same  $\sigma_W$  variation, is shown as the solid curve in Fig. 12. Within 100 pc, where our data anyway are sparse, we still encounter the large variation but beyond  $\sim 100$  pc the derivative and thus the total density seem fairly constant – within only a factor of two.  $\rho_{total}(z \approx 0) \approx 0.05 \mathcal{M}_\odot \text{pc}^{-3}$  between 100 and 200 pc and twice that value at  $\sim 300 - 400$  pc.

### 9. Why does it break down?

We still have not brought the age information into full play. Our attention has been focused on the volume completeness expressed as detectability in a magnitude limited sample and as discussed we have observed all the A stars within  $\sim 450$  pc.

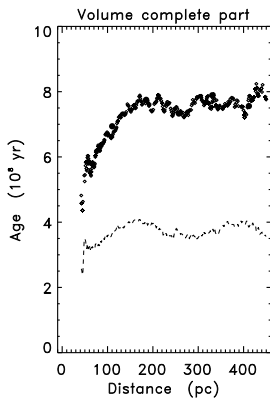


**Fig. 13.** Average age versus  $z$ . Lower curve is the standard deviation. Running 100 pc bins. Filled circles are from the 75 pc independent binning

The observed density variation within this confinement should accordingly approximate the “true” one. The other parameter in Jeans’ equation is the velocity dispersion at a given distance. There may be a relation between dispersion and the distance from the plane as indicated in Fig. 5 but both density and the dispersion may depend on other parameters. There have been several suggestions that dispersions, whatever the reason, increase with time. If there is a  $z$  – age dependence in the sample the  $\nu$  – dispersion comparison has no physical relevance. The discussion in Sect. 6.5 indicated a difference of  $h_{eff}$  and  $\sigma_U$  for the young and old half of the sample. From Table 2 and 3 we recall that  $h_{eff}$  and  $\sigma_U$  were systematically smaller for the younger half, a tendency most pronounced at 150 and 165 pc. A priori we anticipate the young stars to be detected everywhere since they are among the most luminous and with time dependent dynamics a simple requirement is that the mean age does not vary with  $z$ . Fig. 13, mean age versus distance, however shows that this is not the case, filled circles indicate 75 pc independent bins. The age increases homogeneously to about 150 – 200 pc where it levels off and stays constant to the completeness limit at 450 pc. The constant level equals the sample median. The age mix has not matured within 200 pc and the stars on either side of this division can not have experienced comparable dynamical histories. Since Jeans’ equation assumes a high degree of relaxation it may probably not work for the A star sample.

An objection to this is that individual stellar ages are uncertain and cannot be trusted in an absolute way but we may state the same from the distance variation of an accurately observed quantity like the  $\beta$  index. In the A star range  $\beta$  is temperature indicator so it may be replaced by  $(b-y)_0$  but we prefer it since it is unaffected by reddening and less affected by rotation than  $(b-y)_0$ . Fig. 14 shows exactly the same trend as Fig. 13.  $\beta$  varies homogeneously until 200 pc where it becomes constant. 200 pc divides the A stars in two distinct groups. With the distance as the independent parameter we may use the mean age of each distance interval to study the evolution of the U and V dispersions with age(distance). From Fig. 13 we might be led to expect

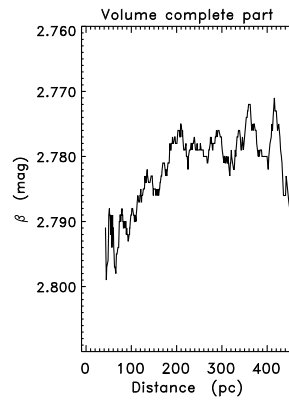


**Fig. 14.** Average  $\beta$  versus  $z$ . Running 100 pc bins. This curve breaks at the same distance where the average age ceases increasing

a homogeneous increase with the age(distance) varying from 5 to  $7.5 \cdot 10^8$  yr and constant values for age(distance)  $\approx 8 \cdot 10^8$  yr.

According to Fig. 15 these expectations are not met. Regarding U the dispersion stays almost constant when the age(distance) increases from  $\sim 4$  to  $\sim 7.5 \cdot 10^8$  yr whereas it displays quite a range  $25 - 45 \text{ km s}^{-1}$  for the constant age(distance)  $\approx 8 \cdot 10^8$  yr. An almost similar variation is noticed for  $\sigma_V$  – age(distance) where the change of behaviour takes place at  $\approx 200$  pc. In Fig. 15c  $\sigma_U$  vs.  $\sigma_V$  is demonstrated, binned by distance. Bins within 200 pc are indicated by  $\square$ ’s and those beyond by  $\diamond$ ’s. The two solid lines indicates that U and V may be heated together following a rather narrow sequence with some wild deviations present. The 200 pc division reveals itself when  $\sigma_V$  becomes constant at  $\sigma_U = 23 \text{ km s}^{-1}$ .

The dispersion – age relations following from the distance binning suggest that  $\sigma_U$  and  $\sigma_V$  may be virtually constant within  $\sim 150$  pc despite the mean age increases with a factor of two. So may we have isothermality after all? In Sect. 10 we present a more detailed discussion of density and kinematics as a function of age and the answer is no!

## 10. Discussion

An interesting question is whether any of Lance’s young high velocity stars observed at the SGP are included in the present bright NGP survey. Since about 1200 square degrees have been observed out to 400 – 700 pc a considerable volume have been sounded so quite a few might be expected. The young high velocity stars was suggested to have exponential scale heights between 1000 and 1600 pc. Their density in the plane may be estimated from Lance (1988) Fig. 7. For scale height 1000 and 1600 pc the expected number within our completeness limit of 450 pc is 10 and 12 respectively, numbers we can not sort out from about 400 stars. For the range 450 – 1300 pc Lance predict 101 young high velocity stars. From the fit of two exponentials ( $h = 65$  and  $165$ ) we predict 68 stars of the kind we have observed, and of these we observe 58. Our simple detection probability is thus  $58/68 = 0.85$ . If the young high velocity stars have the same luminosity distribution as our stars between 450 and 1300 pc we should have seen 86 of the young high velocity

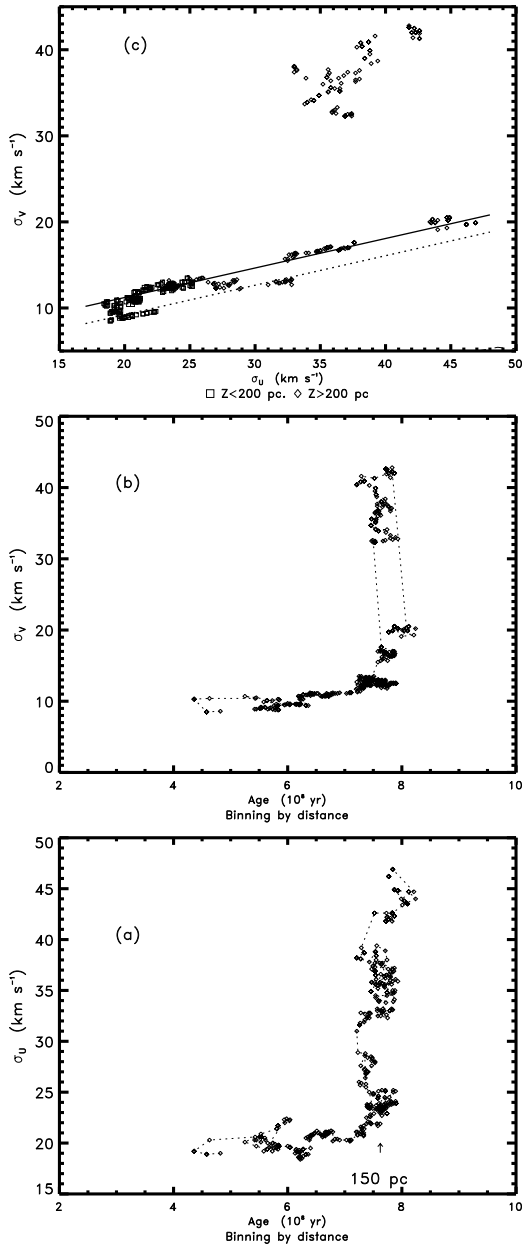


**Fig. 15a–c.** The primary binning is by distance, dispersions and mean ages pertain to a distance bin. **a**  $\sigma_U$  – Age. The turn up is at  $\approx 150$  pc. **b**  $\sigma_V$  – Age. The turn up is at  $\approx 200$  pc indicated by the arrow. **c**  $\sigma_V$  –  $\sigma_U$ .  $\square$ :  $z < 200$  pc,  $\diamond$   $z > 200$  pc

stars alone, but we only observe a total of 68 stars. Is this an indication of a rareness of the young high velocity stars or do they have another luminosity distribution than our “normal” A stars? The fit to the densities resulting from the running bins for the old subgroup required the introduction of a  $\text{sech}^2$  with a scale height 680 pc and we may even have identified some seven individual members of this population. From Sect. 2 we know them to be slightly metal weak, that they have identical masses and luminosities, that they are coeval  $A = 1.0 \pm 0.1$  Gyr but that their planar velocities and dispersions not quite are as extreme as the SGP high velocity stars. These stars may represent another

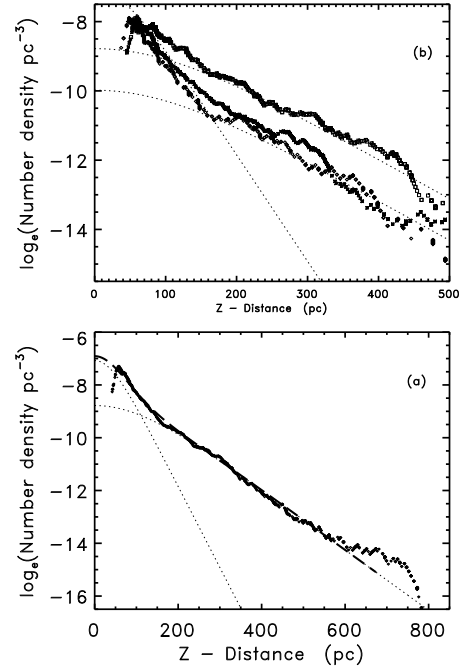


**Fig. 16. a** A two  $\text{sech}^2$  fit to the data. Since there is an age – z variation one might speculate whether two age groups are seen. **b** Density variation of age subgroups, shifted to the density of the 400 – 900  $10^6$  group at 50 pc. Dotted curves are  $\text{sech}^2$  with scale heights 65 and 175 pc included to guide the eye.  $\diamond$ : 0.0 – 0.4 Gyr,  $*$ : 0.4 – 0.9 Gyr,  $\square$ : 0.9 – 1.5 Gyr

family of high altitude A stars than the high velocity population I stars presented by Lance.

The running 100 pc binning made it clear that the density distribution was peculiar between 200 and 300 pc. The formal fit required the introduction of  $\text{sech}^2$ s that do not peak at  $z \approx 0$ . The off plane peaks have concomitant discrepant angular momentum. Such a complex density function does probably not allow an estimate of the total disk density.

The derivative of  $\ln \nu(z)$  showed a complicated variation emphasizing that  $\nu(z)$  is not representing a single or a few isothermals. Between  $\sim 100$  and  $\sim 200$  pc the derivative increases almost linearly, Fig. 11, quite an unexpected behaviour and an effect of the off plane peaks of course. This is only the case when off plane peaks are included, if left out the density variation seems to obey something imitating a sum of two gaussians with scale heights 129 and 250 pc. As it turned out the main reason for the irregularities is a varying age mixture. The average age shows quite different characteristics on either side of 200 pc. Particularly the range  $\sim 100$  and  $\sim 200$  pc is impossible to regard as relaxed since the mean age increases with a factor of two, from  $\sim 4$  to  $8 \cdot 10^8$  yr, over only  $\sim 100$  pc. This age difference has dynamical consequences since it is comparable to what is required for a few orbits around the center and to a minor number of oscillations through the disk, only few relaxing events may have had time to take place. On the other hand stars beyond some hundred pc from the plane are old enough to have approached relaxation. It seems difficult to reconcile the

tracer's varying degree of relaxation with a simple response to the potential. Jeans' equation may not be used to estimate the local mass density.

In our discussion of Fig. 7 we introduced quite a number of curves to match the observations three sech<sup>2</sup>s peaking for  $z=0$  and two peaking at  $z=200$  and  $250$  pc respectively. The resulting match becomes better than 10% at any distance between 50 and 450 pc and differs significantly from the fit in Eq. (1). The physical relevance of all this components may, however, be doubtful. Dividing the sample according to the median age did not change much apart from introducing a curve with scale height 680 pc for the older half. The rather clear variation of the age with  $z$  may suggest that the density variation could be approximated by two curves. Fig. 16a is our best estimate with only two sech<sup>2</sup>s. The fit is inferior to the one in Fig. 7a and does not reproduce the data at 150 pc, where the kink is. Deviation between data and fit is 30% at 150 pc. The proposal could be that  $1.4792 \cdot 10^{-3} \text{ sech}^2(\frac{z}{65})$  might represent a young part of the sample and  $2.6899 \cdot 10^{-4} \text{ sech}^2(\frac{z}{175})$  might reproduce an older population dominating at larger distances but as Fig. 5 and 6a showed the velocity dispersions do not comply with two isothermals but some support for two constituents is lend by the variation of  $\partial \ln \nu / \partial z$  in Fig. 11 and if we accept Eq. (1) the solid curve in Fig. 11 suggests the possible presence of two gaussians. In Fig. 16b we show the density variation for three age groups. Younger than  $400 \cdot 10^6$  yr, between  $400 \cdot 10^6$  and  $900 \cdot 10^6$  and finally those older than  $900 \cdot 10^6$ . The Fig. also contains the two sech<sup>2</sup>s from Fig. 16a. The data are shifted so they match at  $\sim 50$  pc. First we may notice that the relative concentration towards the plane in fact decreases with age as must be the case after Fig. 13 and that at least the two younger subgroups may be approximated by only one curve between  $\sim 70$  and 150 and 200 pc respectively. The oldest group follows a single curve rather well between 150 and  $\sim 400$  pc but we notice that none of the narrow  $\sim 500 \cdot 10^6$  yr age groups may be approximated by just one curve and that the change between curves for the youngest and the oldest age group takes place at the same distance of 150 pc. The changes from one curve to another are particularly extreme for the youngest interval with shifts from a steep curve to a constant between  $\sim 150$  and 210 pc and then to a more shallow curve. An interpretation could be that these young A stars,  $A < 400 \cdot 10^6$  yr, do not share a common origin. But it seems a common characteristic for the three age groups that they are composed of two main features. One feature with a smaller scale height concentrating towards the plane, and most importantly a scale height displaying an increasing tendency with age. For the stars within  $\sim 150$  pc and with  $A < 400 \cdot 10^6$  yr the numerical value of the slope in the  $\log \nu - z$  plane is twice that pertaining to stars with  $A > 900 \cdot 10^6$  yr. This implies that the scale height of the latter is twice that of the former. Increasing the age with  $\approx 1$  Gyr causes a doubling of the scale height. The intermediate age stars obeys consistently a density variation with an intermediate scaleheight within 150 pc. The density variation close to the plane is accordingly not independent of time. The second feature is domineering beyond 150–200 pc and with a larger scale height. The second features are not identical either, we notice

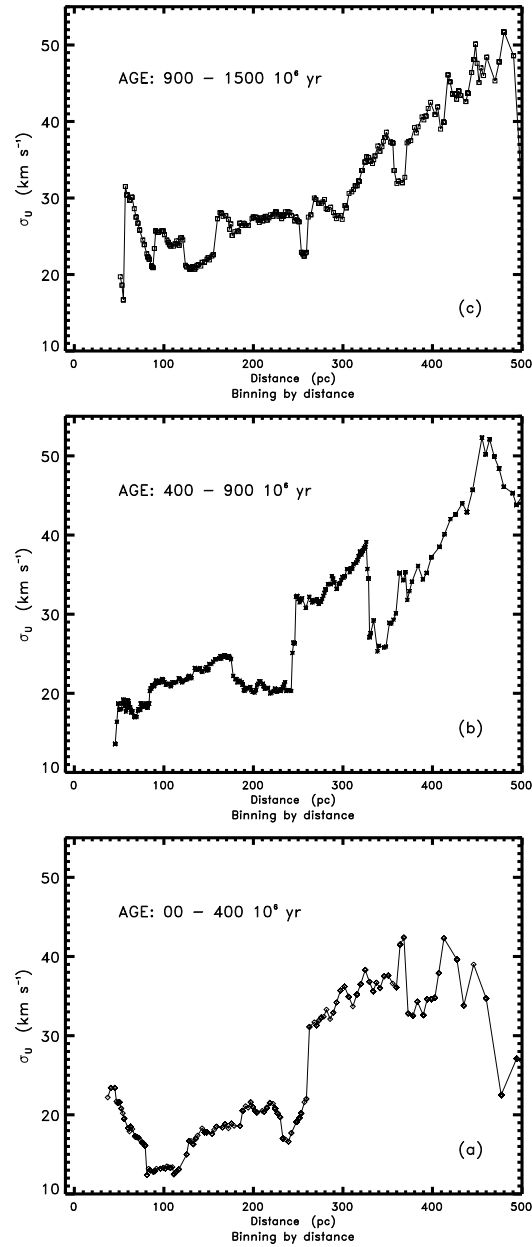


**Fig. 17.**  $\sigma_U$  dispersions for the three age groups of Fig. 16.  $\diamond$ :  $0.0 - 0.4$  Gyr,  $*$ :  $0.4 - 0.9$  Gyr,  $\square$ :  $0.9 - 1.5$  Gyr. 100 pc running distance bins

that the group  $400 - 900 \cdot 10^6$  yr changes slope at  $\approx 300$  pc. The small scale height part is seen to make up a relative diminishing fraction with increasing age. An interpretation might accordingly be that the solar neighborhood has experienced a recent input of stars that have not become old enough to have experienced dynamical relaxation. It is still a problem though why the youngest group does not follow only one density law. There has of course been suggestions that young A stars are results of distinct formation scenarios, Lance (1988). This could be revealed by the variation of velocity dispersion with  $z$ . Fig. 17 shows  $\sigma_U - z$  for our three age groups, distance binning as for Fig. 16. It is interesting to notice that almost all of the fluctuations of the density data have a corresponding variation in  $\sigma_U$ . The most

dramatic feature is the sudden increase and drop of the dispersion noticed for the 400 – 900  $10^6$  yr group at 250 and 350 pc respectively. Returning to the youngest group there is indication that it may consist of two disparate kinematic subgroups dominating on either side of 250 pc with  $\sigma_U \approx 18 \text{ km s}^{-1}$  within 250 pc and  $\sigma_U \approx 35 \text{ km s}^{-1}$  beyond 250 pc. We have coeval stars whose dispersion depends discretely on their distance from the plane. May they have formed under identical circumstances? The two other age groups show a similar behaviour first a low level more or less constant U dispersion – with irregularities – followed by a homogeneous increase to the completeness limit. We recall that  $\partial \ln \nu(z)/\partial z$  from Eq. (1) also indicated a change at  $\sim 200$  pc.

## 11. Conclusions

We propose that, from a 75 pc independent binning, the NGP A stars follow a  $z$  – volume density variation that may be formalized as a sum of four  $\text{sech}^2$  curves, that there is a constant ratio between the W and U dispersions within 375 pc and that the U dispersion increases with  $z$ . The A stars are accordingly not isothermal.

More details may become clearer after changing to overlapping running bins. The formal fit to the density data within the completeness limit by several  $\text{sech}^2$ s of which some do not peak for  $z = 0$  permits the computation of  $\partial \ln \nu(z)/\partial z$  and of  $\partial K_z/\partial z = -\frac{\partial}{\partial z} \left[ \frac{1}{\nu} \frac{\partial}{\partial z} (\nu \sigma_W^2) \right]$  where we have used a linear fit to  $\sigma_W$  over the distance range from 50 to 300 pc.  $\partial \ln \nu(z)/\partial z$  shows that a single isothermal may not be used and  $-\partial K_z/\partial z$  displays a variation amounting to a factor of two in the interval 50 – 130 pc. For larger distances it oscillates and is not confined to positive values. The combination of Poisson's and Jeans' equations is not allowed and may consequently not permit an estimate of the local disk density. If the off plane contributions are left out the  $\partial \ln \nu(z)/\partial z - z$  diagram indicates that the density variations beyond 100 pc imitates a sum of two gaussians with scale heights 129 and 250 pc. Postulating isothermality Bahcall's formalism results in a density estimate  $0.122 \mathcal{M}_\odot \text{ pc}^{-3}$  as calculated between 100 and 200 pc. Including the uncertainty from the fit  $\lesssim 20\%$  the uncertainty in  $\rho_{total}(z \approx 0)$  is about 30%. The density estimate from  $4\pi G \rho = -\partial K_z/\partial z$  indicates an even lower value. The A stars seem thus not to indicate any unidentified matter in the disk.

The absent relaxation may be caused by a varying age with  $z$ . A division of the sample in three age bins have demonstrated that for stars younger than 400  $10^6$  yr  $\sigma_U$  may be approximated by two constant values,  $\sigma_U(z < 250): \sigma_U(z > 250) \approx 18:35$ . Stars with ages between 900 and 1500  $10^6$  yr has a “constant”  $\sigma_U$  within 300 pc and a homogeneously increasing dispersion beyond. The density variation for all three age groups may described coarsely by a sum of two  $\text{sech}^2$ s. Those with the smallest scale heights show an increasing scale height with age and we do not have a steady state. The second components have similar scale heights. The situation is the rather strange that the density variation of the three age groups is reproduced by a sum of two isothermals but the  $z$  variation of their  $\sigma_U$ 's are not those of two

isothermals except perhaps for the youngest subgroup which is made up of stars too short lived to be relaxed in the galactic potential. All three groups contains a hotter remote component.

*Acknowledgements.* My sincere thanks are due to the CAMC for including the NGP stars in the observing programme assuring proper motion completeness. S. Röser, L.V. Morrison and C. Fabricius helped procuring the last 174 proper motions out of a total of 3098, before publication in the CAMC catalogs.

I am indebted to Gerald Gilmore for a thorough criticism of this work.

## References

- Adamson, A.J., Hill, G., Fisher, W., Hilditch, R.W., Sinclair, C.D. 1988 MN 230, 273
- Allen, C.W. 1973, *Astrophysical Quantities*, p. 248
- Bahcall, J.N. 1984a, ApJ 276, 156
- Bahcall, J.N. 1984b, ApJ 276, 169
- Bahcall, J.N., Flynn, C., Gould, A. 1992, ApJ 389, 234
- Carlsberg Meridian Catalogue, La Palma 4 – 8, 1989 – 1994, Copenhagen University Observatory, Royal Greenwich Observatory and Real Instituto y Observatorio de La Armada en San Fernando
- Crawford, D.L. 1979, AJ 84, 1858
- Castellani, V., Cieffy, A., Straniero, O. 1992, ApJS 78, 517
- Dove, J.B., Thronson, H.A. 1993, ApJ 411, 632
- Dworetzky, M.M., Moon, T.T. 1986, MN 222, 787
- Friel, E.D. 1995, Ann.Rev. A&A 33, 381
- Gilden, D.L., Bahcall, J.N. 1985 ApJ 296, 240
- Gould, A. 1990, ApJ 360, 580
- Gould, A., Bahcall, J.N. Flynn, C. 1996 ApJ 465, 759
- Gray, R.O. 1989, ApJS 70, 623
- Green, E.M., Demarque, P., King, C.R. 1987, *The Revised Yale Isochrones and Luminosity Functions* (New Haven: Yale Univ. Obs.)
- Hill, G., Fisher, W.A., Adamson, A.J., Hilditch, R.W., Sinclair, C.D. 1988, PDAO XVI, 297
- Hill, G., Hilditch, R.W., Barnes, J.V. 1979, MN 186, 813
- Just, A., Fuchs, B., Wielen, R., 1996, A&A 309, 715
- Knude, J. 1978, A&AS 33, 347
- Knude, J. 1993a, in Cambridge University Press *Galactic and Solar System Optical Astrometry*, eds. L.V. Morrison and G.F. Gilmore, p. 174
- Knude, J. 1993b, A&A 275, 463
- Knude, J. 1996 A&A 306, 108
- Kuijken, K., Gilmore, G. 1989, MN 239, 651
- Lance, C.M. 1988, ApJ 334, 927
- Marsakov, V.A., Shevelev, Yu.G. 1994, Astron.Rep. 38, 321
- Moon, T.T., Dworetzky, M.M. 1985, MN 217, 305
- Perry, C.L. 1969, AJ, 74, 139
- Palouš, J., Piskunov, A.E. 1985 A&A 143, 102
- Preston, G.W., Beers, T.C., Schectman S.A. 1994, AJ 108, 538
- Rodgers, A.W., Roberts, W.H. 1993a, AJ 106, 1839
- Rodgers, A.W., Roberts, W.H. 1993b, AJ 106, 2294
- Röser, S., Bastian, U. 1993, BCDA 42, 11
- Smalley, B., Dworetzky 1993, ASP Conference Series 44, 182
- Strömgren, B. 1966, Ann.Rev. A&A 4, 434
- van der Kruit, P.C. 1988, A&A 192, 117
- van der Kruit, P.C., Searle, L. 1981, A&A 95, 105
- This article was processed by the author using Springer-Verlag L<sup>A</sup>T<sub>E</sub>X A&A style file L-AA version 3.